Nucleic Acids Research, 2025, **53**, gkae1291
https://doi.org/10.1093/nar/gkae1291
Advance access publication date: 11 January 2025
Genome integrity, repair and replication

Negative DNA supercoiling enhances *DARS2* binding of DNA-bending protein IHF in the activation of Fis-dependent ATP-DnaA production

Kazutoshi Kasho *, Kenya Miyoshi, Mizuki Yoshida, Ryuji Sakai, Sho Nakagawa and Tsutomu Katayama

Department of Molecular Biology, Graduate School of Pharmaceutical Sciences, Kyushu University, Fukuoka 812-8582, Japan
*To whom correspondence should be addressed. Tel: +81 92 642 6644; Fax: +81 92 642 6646; Email: kazutoshi.kasho@phar.kyushu-u.ac.jp

Abstract

Oscillation of the active form of the initiator protein DnaA (ATP-DnaA) allows for the timely regulation for chromosome replication. After initiation, DnaA-bound ATP is hydrolyzed, producing inactive ADP-DnaA. For the next round of initiation, ADP-DnaA interacts with the chromosomal locus *DARS2* bearing binding sites for DnaA, a DNA-bending protein IHF, and a transcription activator Fis. The IHF binding site is about equidistant between the DnaA and Fis binding sites within *DARS2*. The *DARS2*-IHF-Fis complex promotes ADP dissociation from DnaA and furnishes ATP-DnaA at the pre-initiation stage, which dissociates Fis in a negative-feedback manner. However, regulation for IHF binding as well as mechanistic roles of Fis and specific DNA structure at *DARS2* remain largely unknown. We have discovered that negative DNA supercoiling of *DARS2* is required for stimulating IHF binding and ADP dissociation from DnaA *in vitro*. Consistent with these, novobiocin, a DNA gyrase inhibitor, inhibits *DARS2* function *in vivo*. Fis Gln68, an RNA polymerase-interaction site, is suggested to be required for interaction with DnaA and full *DARS2* activation. Based on these and other results, we propose that DNA supercoiling activates *DARS2* function by stimulating stable IHF binding and DNA loop formation, thereby directing specific Fis–DnaA interaction.

Graphical abstract

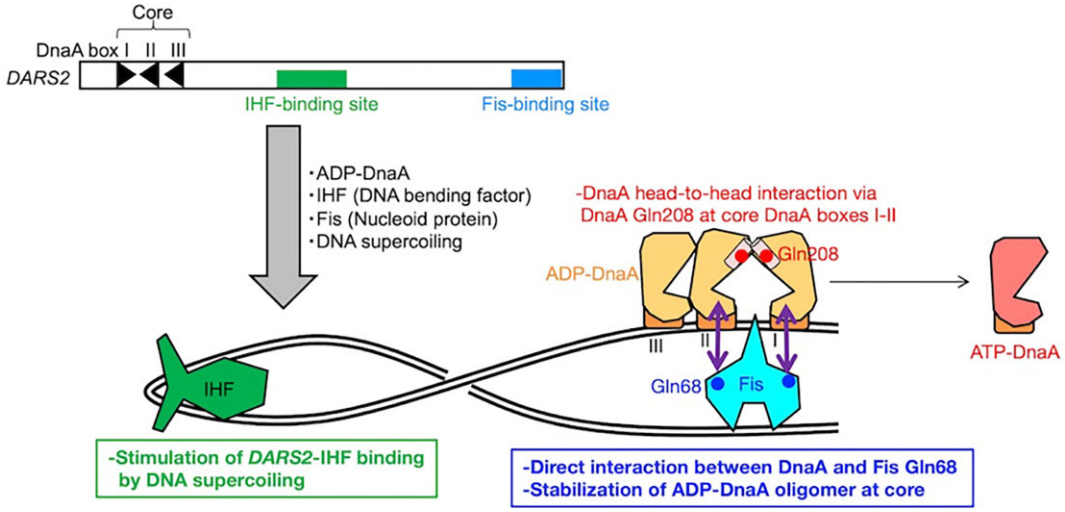

Introduction

Bacterial chromosomes form a condensed nucleoid structure by binding nucleoid-associated proteins (NAPs) and forming DNA supercoils which are controlled by DNA topoisomerases, local transcription, etc. (1–3). The timing of *E. coli* chromosomal replication is tightly regulated to be initiated at the replication origin *oriC* once per cell cycle in a manner coordinated with growth environments (Figure 1A) (4–6). The initiator protein DnaA binds to *oriC* and promotes initiation, which is regulated by supercoiling of DNA and NAPs. However, underlying mechanisms remain to be investigated.

Received: August 9, 2024. **Revised:** December 13, 2024. **Editorial Decision:** December 13, 2024. **Accepted:** December 19, 2024

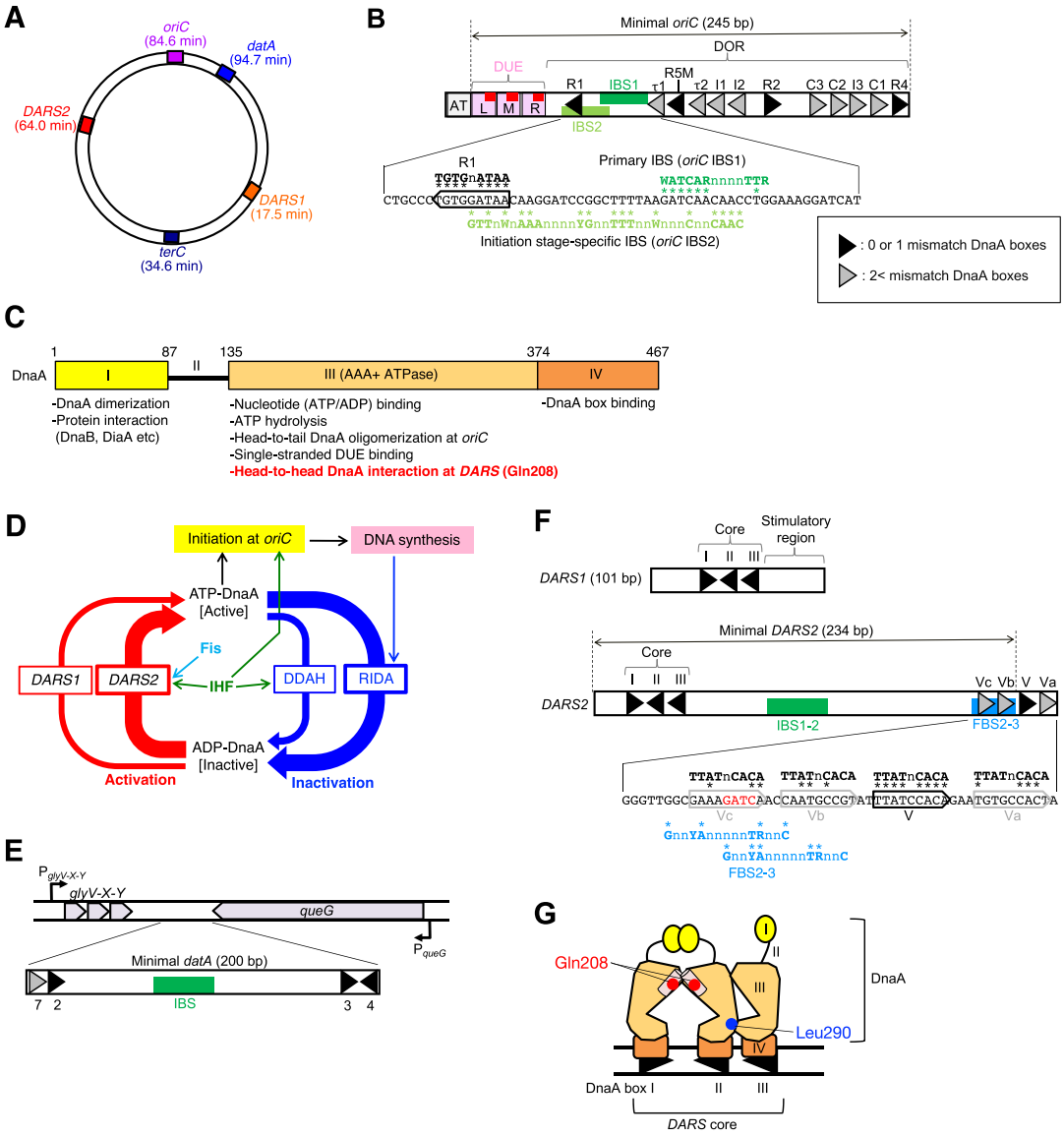

Figure 1. Structures of *oriC*, *datA*, *DARS1*, and *DARS2*. (**A**) Schematic representation of the genomic DNA elements *oriC*, *datA*, *DARS1*, *DARS2*, and *terC* on the 4.6 Mb circular *E. coli* chromosome. (**B**) Structure of *oriC*. The open bar indicates *oriC* (250 bp) including the DOR, the DUE and the AT-cluster (AT) (23). DOR includes 9-mer DnaA boxes (triangles), primary IBS (IBS1) and the initiation stage-specific secondary IBS (IBS2), which overlaps with the DnaA box R1. DUE includes the 13-mer elements and DnaA binding sequences TTRT(T) (R indicates A or G), which binds DnaA in a single-stranded form. The AT-cluster assists in DUE unwinding in specific conditions. (**C**) Domains of DnaA and their function. The major roles of each domain (domain I, III, and IV) are summarized. (**D**) Schematic presentation of the regulatory cycle of DnaA. ATP-DnaA initiates DNA replication from *oriC* with the aid of IHF. ATP-DnaA is converted to ADP-DnaA by RIDA and DDAH systems. RIDA requires the complex of Hda protein and the DNA-loaded form of clamp subunit of DNA polymerase III holoenzyme, and DDAH requires the *datA*-IHF complex. *DARS1* and *DARS2* loci stimulate nucleotide exchange of ADP-DnaA to produce ATP-DnaA. *DARS2*-dependent ATP-DnaA production requires IHF and Fis. (**E**) A schematic presentation of the chromosomal *datA* locus. tRNA and protein coding regions (*glyV-X-Y* and *queG*, respectively) are indicated. Bent arrows indicate transcriptional promoters ($P_{glyV\text{-}X\text{-}Y}$ and P_{queG}). The minimal *datA* (200 bp) consists of DnaA boxes 2, 3, 7 and 4 and a single IBS. The *datA* DnaA boxes 2, 3 and 7 are essential and DnaA box 4 is stimulatory for DDAH. (**F**) Structures of *DARS1* and *DARS2*. The upper and lower open bars indicate *DARS1* (101 bp) and *DARS2* (256 bp), respectively. *DARS1* and *2* share oppositely oriented DnaA boxes I and II, and DnaA box III. This region is termed Core and is essential for DnaA-ADP dissociation. IBS1-2 and FBS2-3 are also essential for *DARS2* activation. The ATP-DnaA-specific, low-affinity DnaA boxes Va, Vb, and Vc, that partly overlap with FBS2–3, are shown. (**G**) ADP-DnaA oligomerization at *DARS* core DnaA boxes. Three molecules of ADP–DnaA bind to Core DnaA boxes I, II, and III. DnaA molecules bound to DnaA boxes I and II physically interact via Gln208 residue in AAA + domain III in a head-to-head manner, whereas DnaA molecules bound to DnaA boxes II and III interact via Leu290 residue in AAA + domain III in a head-to-tail manner.

oriC consists of a duplex-unwinding element (DUE), and a flanking DnaA oligomerization region (DOR) composed of clusters of DnaA boxes, which are specific 9-mer sequences for DnaA binding and have the consensus of TTATnCACA (n is any nucleotide) (Figure 1B). Also, IHF, a NAP, sequence-specifically binds to DOR (Figure 1B). IHF consists of a heterodimer of α- and β-subunits (3), and specifically binds to IBS (IHF-binding site) with the consensus sequence of YAAnnnnTTGATW (where Y is C or T, and W is A or T), inducing sharp DNA bending and topological constraint (7,8).

DnaA consists of four functional domains (Figure 1C) (9–12). Domain I functions as an interaction hub for various proteins such as DnaB helicase and DnaA-assembly factor DiaA (13–15). Domain II is a flexible linker (13,16). Domain III is a AAA + ATPase domain for ATP/ADP binding, ATP hydrolysis, DnaA–DnaA interactions, and single-stranded DUE binding (Figure 1B and C) (9–12). Domain IV specifically binds to DnaA box sequences (17).

Initiation-active ATP-DnaA forms head-to-tail oligomers at *oriC* DOR, which is stimulated by DiaA (18–20). The ATP–DnaA complexes induce transient DUE unwinding of supercoiled *oriC*, which is stimulated by IHF binding (21) and stabilized by the sequence-specific interaction of the single-stranded DUE with DOR-bound DnaA (22–24). DnaB helicases are loaded to the stably unwound DUE, followed by construction of replisomes.

The cellular ATP-DnaA level fluctuates during the cell cycle and peaks at the time of replication initiation (25). After initiation, the regulatory inactivation of DnaA (RIDA) system immediately hydrolyzes DnaA-bound ATP to produce initiation-inactive ADP-DnaA (Figure 1D) (26–29). RIDA is backed up by the DDAH (*datA*-dependent DnaA-ATP Hydrolysis) system (Figure 1D) (30,31). The minimal *datA* region for DDAH contains four DnaA boxes and a single IBS (Figure 1A and E) (31). The *datA*-IHF complex catalytically promotes DnaA-ATP hydrolysis and produces ADP-DnaA. We previously suggest that IHF induces DNA loop formation and promotes the key interactions between the ATP-DnaA oligomers for the activation of ATP hydrolysis. IHF binds to *datA* specifically after initiation, ensuring the timely activation of DDAH (30). The *datA*-IHF binding is regulated by negative DNA supercoiling and transcription of the *datA*-proximal tRNA-Gly (*glyV-X-Y*) operon (Figure 1E) (31,32).

In the pre-initiation stage, ADP-DnaA is converted to ATP-DnaA by chromosomal DnaA Reactivating Sequence (DARS) *1* and *2* that share specific core DnaA boxes I, II and III (Figure 1A, D and F) (33,34). *In vivo*, *DARS2* is predominant for ATP-DnaA production, while *DARS1* is supportive. Unlike the head-to-tail arrangement of *oriC* DnaA boxes, the *DARS* core DnaA boxes I and II have a head-to-head arrangement and induce head-to-head ADP-DnaA interaction that dissociate ADP (Figure 1G) (33,35). *DARS* core DnaA box III plays an essential role for the *DARS* function by enhancing DnaA oligomer formation. *DARS1* does not require any protein activators (33,35). By contrast, *DARS2* core DnaA boxes are less active for DnaA-ADP dissociation and are drastically activated by specific binding of IHF and another NAP Fis to IBS1-2 and FBS2-3 (Fis-binding sites 2–3), respectively (Figure 1F) (34). Fis is abundant in log-phase cells, and forms a homodimer, which specifically binds to the consensus sequence GnnYAnnnnTRnnC, inducing slight DNA curvature (3,36). However, the molecular mechanism of *DARS2* activation by IHF and Fis remains unclear.

In addition, *DARS2* activity is regulated by the timely binding of IHF and Fis in the pre-initiation stage for chromosome replication (34,37). At the initiation stage, ATP-DnaA molecules are abundant and cooperatively construct oligomers in *DARS2* DnaA box V and its flanking low-affinity DnaA boxes, which overlap with FBS2-3 (Figure 1F), competitively dissociating Fis from FBS2-3 as a negative feedback (37). By contrast, regulation for IHF binding at *DARS2* still remains to be investigated.

This study reports that negative DNA supercoiling supports *DARS2* activation by stimulating stable binding of IHF to *DARS2 in vitro*. Consistently, DNA supercoiling is suggested to activate *DARS2 in vivo*. Mutational analyses of Fis support an idea that Fis site-specifically interacts with DnaA for activating *DARS2*. Based on these and other results, we propose that DNA supercoiling is a prerequisite for stable IHF binding and DNA bending in *DARS2*, which conformationally stimulate functional interaction between *DARS2*-bound DnaA and Fis.

Materials and methods

Proteins, DNA and *E. coli* strains

DnaA and IHF were purified as described previously (23,38). For constructing overproducers of C-terminally His_6-tagged Fis mutants (Q68A, T70A, Δ16–22 and Δ26), the mutations were induced by inverse PCR using pET-Fis6H(WT) as a template and the following primers (Supplementary Tables S1 and S2): MK-102 and MK-103 for Fis Q68A, MK-102 and MK-105 for Fis T70A, MK-110 and MK-111 for Fis Δ16–22 and MK-112 and MK-116 for Fis Δ26. As described, the His_6-tagged Fis protein was overexpressed in BL21(λDE3) cells transformed with its overproducer by adding 1.0 mM IPTG. The protein was purified using Ni^{2+}-NTA agarose column chromatography. The purity of each protein was > 90% as judged by SDS-PAGE and Coomassie Brilliant Blue staining.

Plasmids pOA61 and pOA21 are pACYC177-derivatives bearing *DARS2* WT and *DARS1* WT, as described previously (33,34). pOA61 derivatives harboring *DARS2* sequence substitutions were constructed by inverse PCR using the following primers (Supplementary Tables S1 and S2): D2I12EcoRV-U and D2I12EcoRV-L for pKX137 [*DARS2* IBS1-2-EcoRV], pOA61BclI-U and pOA61BclI-L for pKX141 [*DARS2* FBS2-3-BclI], KshD2-1 and KshD2-2 for pKX115 [*DARS2*exDnaAboxI], KshD2-4 and KshD2-5 for pKX117 [*DARS2*exDnaAboxII], KshD2-4 and KshD2-6 for pKX118 [*DARS2*exDnaAboxIII], KshD2-1 and KshD2-7 for pKX119 [*DARS2*exCore] and KshD2-5 and KshD2-12 for pKX129 [*DARS2*exDnaAboxI-II]. Linear forms (Lin) of pOA61, pACYC177, pOA21, pOA76 [*DARS1*ΔCore], pKX137, pKX141 and pKX129 were prepared by SacII digestion and purified using the Wizard SV Gel and PCR Clean-Up System (Promega) or NucleoSpin® Gel and PCR Clean-up (Macherey-Nagel). Relaxed forms (Relax) of pOA61was prepared by incubation with DNA Topoisomerase I (Takara) and were purified using Wizard SV Gel and PCR Clean-Up System (Promega). pOA61tet-derivatives for λ Red recombination, as described below, were similarly constructed using the following primers (Supplementary Table S1): KshD2-1 and KshD2-2 for pKX115tet [*DARS2*exDnaAboxI-*tet*], KshD2-4 and KshD2-5 for pKX117tet [*DARS2*exDnaAboxII-*tet*], KshD2-4 and KshD2-6 for pKX118tet [*DARS2*exDnaAboxIII-*tet*],

Table 1. List of *E. coli* strains used in this study

Strain	Genotype	Source
MG1655	WT	Laboratory stock
DH5α	*supE44ΔlacU169(φ80lacZΔM15) hsdR17 recA1 endA1 gyrA96 thi-1 relA1*	Laboratory stock
BL21(DE3)	F⁻*ompT hsd*SB(r_B^-, m_B^-) *gal dcm* (DE3)	Laboratory stock
MIT17	MG1655 *DARS1ΔCore::kan*	(33)
MIT78	MG1655 *DARS2ΔCore::cat*	(33,34,48)
MIT80	MG1655 *DARS1ΔCore::kan DARS2ΔCore::cat*	(33,34)
MIT128	MG1655 *ΔdatA::cat*	(31)
KMG-5	MG1655 *ihfA::frt-kan*	(34)
KMG-2	MG1655 *fis::frt-kan*	(34)
KX219	MG1655 *DARS2*exDnaAboxII-*tet*	This work
KX221	MG1655 *DARS2*exCore-*tet*	This work
KX222	MG1655 *DARS2*exDnaAboxI-II-*tet*	This work

KshD2-1 and KshD2-7 for pKX119tet [*DARS2*exCore-*tet*], and KshD2-5 and KshD2-12 for pKX129tet [*DARS2*exDnaAboxI-II-*tet*], respectively.

Oligonucleotides listed in Supplementary Table S1 for the electrophoretic mobility shift assay (I12U and I12L for *DARS2* IBS1-2 WT; D2I12EcoRV-U and D2I12EcoRV -L for *DARS2* IBS1-2-EcoRV; F23U and F23L for *DARS2* FBS2-3 WT; FBS23BclI-U and FBS23BclI-L for *DARS2* FBS2-3-BclI; subF23U and subF23L for *DARS2* subFBS2-3 WT; D2DI-U and D2DI-L for *DARS2* DnaA box I; D1DI-U and D1DI-L for *DARS1* DnaA box I; D2DII-U and D2DII-L for *DARS2* DnaA box II; D1DII-U and D1DII-L for *DARS1* DnaA box II; D2DI-II-U and D2DI-II-L for *DARS2* DnaA box I-II; and D1DI-II-U and D1DI-II-L for *DARS1* DnaA box I-II, respectively) were annealed at room temperature overnight after boiling.

All *E. coli* strains used in this study are listed in Table 1. As described previously, chromosomal *DARS2* mutants were introduced in MG1655 cells harboring pKD46 (39); DNA fragments carrying the *DARS2* mutation and *tet* gene were amplified using pKX117tet for KX219 [*DARS2*exDnaAboxII], pKX119tet for KX221 [*DARS2*exCore] and pKX129tet for KX222 [*DARS2*exDnaAboxI-II], respectively.

In vitro reconstitution of *DARS2* DnaA-ADP dissociation

As described previously (34,35), [^{3}H]ADP-DnaA was prepared by incubation of nucleotide-free DnaA at 0°C for 15 min in buffer N (50 mM Hepes-KOH [pH 7.6], 2.5 mM magnesium acetate, 0.3 mM EDTA, 7 mM dithiothreitol, 20%(v/v) glycerol, and 0.007%(v/v) Triton X-100) containing 3 μM [^{3}H]ADP. The resultant [^{3}H]ADP-DnaA (80 nM) was incubated in 25 μL of reaction buffer (20 mM Tris-HCl [pH 7.5], 100 mM potassium glutamate, 10 mM magnesium acetate, 2 mM ATP, 8 mM dithiothreitol, and 100 μg/mL bovine serum albumin) containing 150 ng poly(dI-dC) and indicated amounts of *DARS2* (Sc, Lin, or Relax), IHF and Fis. Then, DnaA-bound [^{3}H]ADP was recovered on nitrocellulose filters, and quantified in a liquid scintillation counter.

Electrophoretic mobility shift assay

Indicated amounts of DnaA, IHF, or Fis were incubated with double-stranded DNA at 30°C for 5 min in 10 μL of reaction buffer containing 100 mM potassium glutamate and the indicated amounts of poly(dI-dC) or lambda DNA as competitors, followed by analysis by 7–10% PAGE at 100 V for 60–80 min in Tris-Borate buffer and staining with GelStar or GelRed.

Restriction enzyme protection assay for IHF/Fis binding

For the analysis of *DARS2*-IHF binding using the PciI protection assay, linear or supercoiled plasmid pOA61 [*DARS2* WT] (0.4 nM) was incubated at 30°C for 5 min with various amounts of IHF in 10 μL of reaction buffer containing 100 mM NaCl followed by further incubation at 30°C for 5 min with PciI (New England BioLabs, 0.4 units). The reaction was terminated by adding SDS loading buffer, and DNA fragments were analyzed by 1% (w/v) agarose gel electrophoresis. For the analysis of *DARS2*-IHF binding by the EcoRV protection assay, the plasmid pKX137 [*DARS2* IBS1-2-EcoRV] (0.4 nM), which contains a *DARS2* sequence engineered to contain a EcoRV recognition site in IBS1-2, was used. For the analysis of *DARS2*-Fis binding by the BclI protection assay, the plasmid pKX141 [*DARS2* FBS2-3-BclI] (0.4 nM), which contains a *DARS2* sequence engineered to contain a BclI-recognition site in FBS2-3, was used.

Protein crosslinking assay

For the analysis of direct Fis-DnaA interaction, 100 nM of ADP-DnaA and 0–200 nM of Fis WT or Q68A were incubated at 30°C for 15 min in the presence of 0.1% glutaraldehyde in 20 μL of reaction buffer containing 100 mM NaCl. *DARS2* DNA was not added in the crosslinking assay. The reaction was terminated by adding 10% trichloroacetic acid, and precipitated proteins were analyzed by SDS-12% PAGE and immunoblotting using anti-Fis antibody.

Flow cytometry

As described previously, cells were cultivated at 37°C in LB medium (with or without NaCl) or supplemented M9 medium in the presence or absence of 100 μg/mL ampicillin or 15 μg/mL novobiocin until an A_{660} (absorbance at 660 nm) of 0.1–0.2 was reached, followed by further incubation at 37°C for 4 h in the presence of 300 μg/mL rifampicin and 10 μg/mL cephalexin for run-out replication. The resultant cells were fixed with 70% ethanol, stained with SYTOX Green (Life Technologies), and analyzed with FACS Calibur (BD Biosciences).

Results

Negative DNA supercoiling stimulates DnaA-ADP dissociation by the *DARS2*-IHF-Fis complex *in vitro*

First, to examine whether negative DNA supercoiling is required for *DARS2*-dependent DnaA-ADP dissociation, [^{3}H]ADP-bound DnaA was incubated with supercoiled plasmid harboring *DARS2*, termed pOA61 (pACYC177-*DARS2*), its SacII-digested linear DNA derivative, or its parental plasmid pACYC177 (Figure 2A), followed by quantification of DnaA-bound [^{3}H]ADP by the filter binding assay. In the standard *in vitro DARS2* reconstitution assay containing 2 nM each of IHF and Fis as dimers (34), supercoiled but not linear pOA61, efficiently dissociated DnaA-bound [^{3}H]ADP from DnaA (Figure 2B). Under the same experimental conditions, neither supercoiled nor linear pACYC177 showed substantial DnaA-ADP dissociation activity. Consistent with the requirement for DNA supercoiling, little or no DnaA-ADP dissociation activity was observed when pOA61 supercoiling was relaxed by DNA Topoisomerase I (Figure 2A, C and D). These

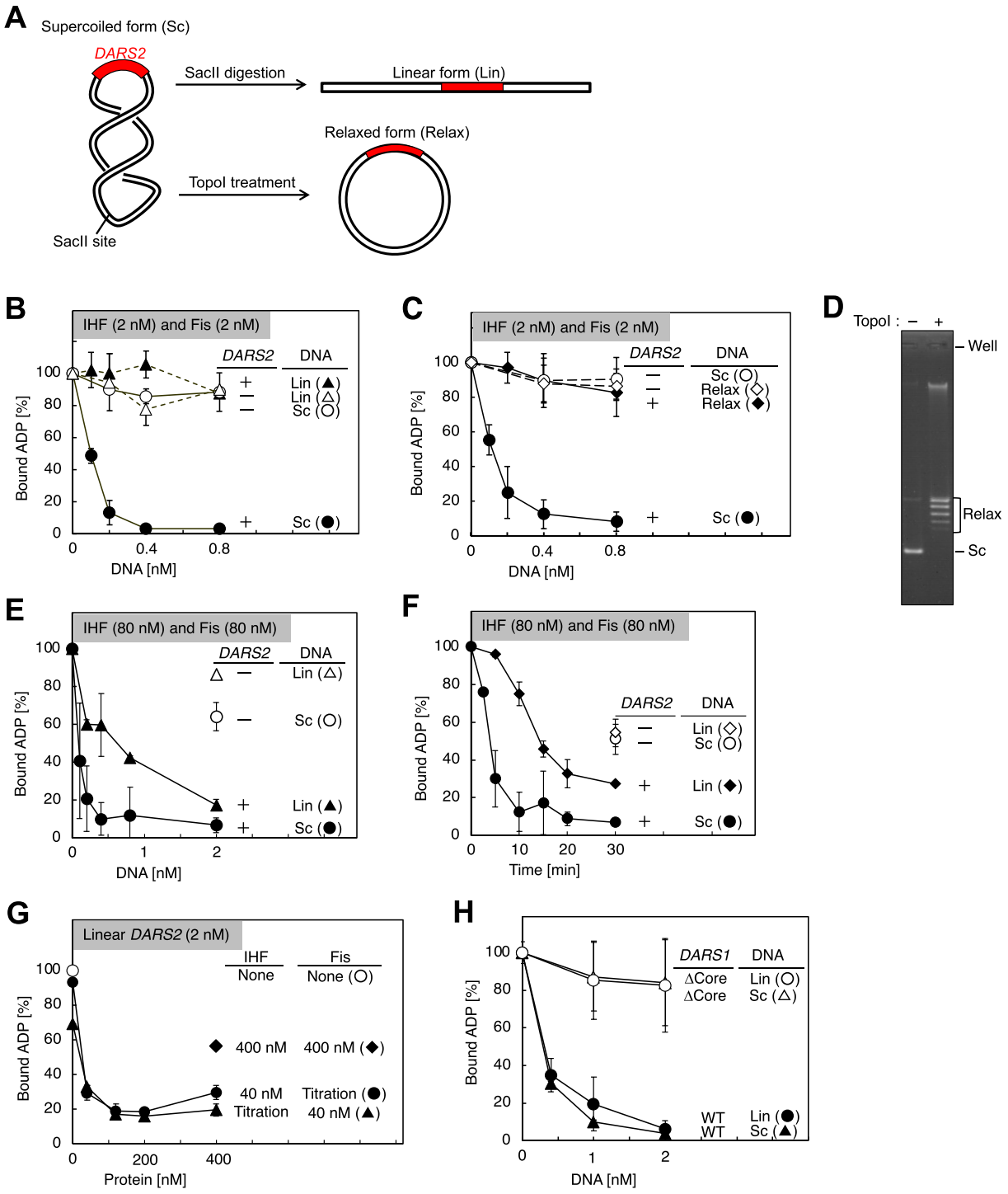

Figure 2. DNA supercoiling-dependent activation of *DARS2* DnaA-ADP dissociation. (**A**) Structure and preparation of supercoiled (Sc), linear (Lin), and relaxed (Relax) forms of *DARS2*-plasmids. pOA61, a pACYC177-based plasmid harboring the *DARS2* WT fragment (991 bp), was used for analysis of DnaA-ADP dissociation (33,34). Linear pOA61 was prepared by digestion using restriction enzyme SacII. Relaxed pOA61 was prepared by Topoisomerase I (TopoI) treatment. (**B**) Comparison of DnaA-ADP dissociation activity with supercoiled or linear *DARS2*. [^{3}H]ADP-DnaA (80 nM) was incubated at 30°C for 15 min with IHF (2 nM as heterodimer), Fis (2 nM as homodimer), and the indicated amounts of the supercoiled (Sc) or linear forms (Lin) of pOA61 or pACYC177, followed by a filter binding assay to analyze the yield amount [%] of [^{3}H]ADP-DnaA. Average values and the errors from at least two independent experiments are shown. (**C, D**) Comparison of DnaA-ADP dissociation activity with supercoiled or relaxed *DARS2*. The supercoiled or relaxed forms (Relax) of pOA61 or pACYC177 were similarly analyzed (**C**). For preparing the relaxed form, supercoiled pOA61 was incubated with Topoisomerase I. The products were analyzed using 0.65% (w/v) agarose gel electrophoresis, and ethidium bromide staining (**D**). (**E-G**) The DnaA-ADP dissociation activity of linear *DARS2* in the presence of excess IHF and Fis. Filter binding assay was performed with IHF (80 nM), Fis (80 nM) and the indicated amounts of pOA61 or pACYC177 (Sc or Lin) (**E**). [^{3}H]ADP-DnaA (80 nM) was incubated at 30°C for indicated times with IHF (80 nM), Fis (80 nM), and 0.8 nM of pOA61 or pACYC177 (Sc or Lin) (**F**). Similar experiments were performed in the presence of indicated amounts of IHF or Fis (**G**). (**H**) Supercoiling-independent activity of *DARS1*. Filter binding assay was performed with the indicated amounts of pOA21 [*DARS1* WT] or pOA76 [*DARS1*ΔCore] (Sc or Lin).

results indicate that *DARS2*-dependent DnaA-ADP dissociation requires DNA supercoiling *in vitro*.

To test further how DNA supercoiling affects the functions of IHF and Fis required for *DARS2* activation, an *in vitro DARS2* reconstitution assay was performed in the presence of excessive amounts of IHF and Fis. Unlike under standard conditions (2 nM each of IHF and Fis), these assays containing 80 nM each of IHF and Fis moderately stimulated DnaA-ADP dissociation with linear pOA61 (Figure 2E), whereas the level of DnaA-ADP dissociation with supercoiled pOA61 in these assays was comparable to that in the standard assay (Figure 2B and E). These results suggest that DNA supercoiling is stimulatory, but not essential, for IHF/Fis functions in *DARS2*. This idea was supported by the results of the time course experiments (Figure 2F). Quantitative analysis of DnaA-ADP dissociation in the presence of various amounts of IHF and a fixed amount (40 nM) of Fis or *vice versa* indicated that 40 nM each of IHF and Fis was sufficient to promote DnaA-ADP dissociation with linear pOA61 (Figure 2G). In contrast to *DARS2*, DNA supercoiling did not stimulate *DARS1*-dependent DnaA-ADP dissociation, which does not require IHF or Fis (Figure 2H), suggesting that DNA supercoiling stimulates the functions of IHF and Fis rather than ADP-DnaA oligomerization at the core DnaA boxes.

IHF and Fis activate a *DARS2* mutant harboring *DARS1* core DnaA boxes in a manner dependent on DNA supercoiling

To test the hypothesis that IHF and Fis regulate the conformational changes of ADP-DnaA oligomers occurring at core DnaA boxes in a manner dependent on DNA supercoiling, we first analyzed ADP-DnaA binding to each DnaA box of *DARS1* and *DARS2*. DnaA box II of *DARS1* only has the complete match to the consensus and others have a different single mismatch to the consensus (Figure 3A). In EMSA using linear 19-bp DNA containing a single DnaA box, ADP-DnaA efficiently formed a discrete complex on *DARS1* DnaA box I DNA, whereas it did not on *DARS2* DnaA box I DNA, as evidenced by the absence of a discrete band shift (Figure 3B), demonstrating that ADP-DnaA has higher affinity for *DARS1* DnaA box I DNA than for *DARS2* DnaA box I DNA. In contrast to *DARS2* DnaA box I, ADP-DnaA formed a discrete complex on *DARS2* DnaA box II; however, the ADP-DnaA binding affinity for the *DARS2* DnaA box II was significantly lower than that for *DARS1* core DnaA box II which has the complete consensus sequence (Figure 3C). Next, we performed EMSA using linear DNA fragment containing two oppositely oriented DnaA boxes I–II (Figure 3D). Consistent with the ADP-DnaA binding affinities for each DnaA box, *DARS1* core DnaA boxes I-II formed ADP-DnaA oligomers more efficiently than *DARS2* core DnaA boxes I-II.

Next, to analyze DnaA box-dependent ADP dissociation activity in supercoiled and linear DNA, the set of the DnaA boxes I-II of *DARS2* was exchanged with those of *DARS1*, resulting in *DARS2*exDnaAboxI-II mutant (Figure 3A). DnaA-ADP dissociation activity of supercoiled or linear DNA bearing *DARS2*exDnaAboxI-II in the absence or presence of IHF and Fis, was compared it with that of *DARS1* or *DARS2* WT under the same conditions (Figure 3E). Interestingly, the linear *DARS2*exDnaAboxI-II mutant DNA sustained comparable DnaA-ADP dissociation activity to that of the linear *DARS1* DNA. Also, DnaA-ADP dissociation activity with supercoiled pKX129 [*DARS2*exDnaAboxI-II] was stimulated by the addition of 2 nM each of IHF and Fis in a manner dependent on DNA supercoiling (Figure 3F). These results indicate that IHF and Fis can stimulate *DARS1* core-dependent DnaA-ADP dissociation in a manner dependent on DNA supercoiling even though the core DnaA boxes harbor higher activity than that of the *DARS2* core. This implies a possibility that either IHF or Fis directly interacts with ADP-DnaA oligomers formed at the *DARS* core for optimizing complex conformation.

DNA supercoiling stimulated stable binding of IHF, but not Fis, to *DARS2*

To assess whether negative DNA supercoiling stabilizes IHF/Fis binding within *DARS2*, a restriction enzyme protection assay was performed in the presence of 100 mM NaCl (Figure 4). The plasmid pOA61 carries a single PciI recognition sequence 5′-ACATGT-3′ (Figure 4A), which partly overlaps with the *DARS2* IBS1-2 region protected in DNase I footprint experiments (34). In the absence of IHF, both the supercoiled and linear forms of pOA61 were digested by PciI with similar efficiency (Figure 4B). In the PciI protection assay, supercoiled or linear pOA61 was incubated with or without IHF, followed by further incubation with a fixed amount of PciI (0.4 units/sample for Sc or Lin pOA61). The results showed that addition of IHF inhibited PciI digestion of pOA61 in a manner dependent on DNA supercoiling (Figure 4C and D), indicating that IHF preferentially binds to *DARS* IBS1-2 on supercoiled DNA rather than to that on linear DNA. Similar experiments were performed using EcoRV, which was originally used to analyze whether DNA supercoiling stabilizes the *datA*–IHF complex (31). Both the supercoiled and linear forms of *datA* plasmid are digested by EcoRV with similar efficiency in the absence of IHF (31). Accordingly, we introduced the EcoRV recognition sequence 5′-GATATC-3′ at *DARS2* IBS1-2 to generate plasmid pKX137 [*DARS2* IBS1-2-EcoRV] (Figure 4E). EMSA experiments using 38-bp *DARS2* IBS1-2 fragments indicated that IHF binding activity was little affected with the *DARS2* IBS1-2-EcoRV mutation (Figure 4F). IHF inhibited EcoRV digestion (0.5 units/samples for Sc or Lin pKX137) of pKX137 in a manner dependent on DNA supercoiling (Figure 4G), consistent with the results of the PciI protection assay (Figure 4D). These results conclusively support the idea that DNA supercoiling affects IHF binding to *DARS* IBS1-2 and stabilizes the IHF–DNA complex.

Furthermore, we assessed whether DNA supercoiling stimulates *DARS2*-Fis binding (Figure 4H). The BclI recognition sequence 5′-TGATCA-3′ was introduced at *DARS2* FBS2-3 without changing the consensus sequences to generate plasmid pKX141 [*DARS2* FBS2-3-BclI] (Figure 4H). EMSA experiments indicated that Fis binding activity was little affected with the FBS2-3-BclI mutation (Figure 4I). In the absence of Fis, supercoiled pKX141 was digested more efficiently by BclI than linear pKX141 (Figure 4J). For this reason, we employed different amounts of BclI (1.2 units/sample for supercoiled pKX141, and 3.0 units/sample for linear pKX141) in the BcII protection assay to equalize the activity to each substrate and determined whether DNA supercoiling affects *DARS2*-Fis binding. Fis inhibition of BclI digestion was little affected by pKX141 DNA structure (Figure 4K), indicating that DNA supercoiling does not stabilizes *DARS2* binding to Fis, unlike the situation with IHF.

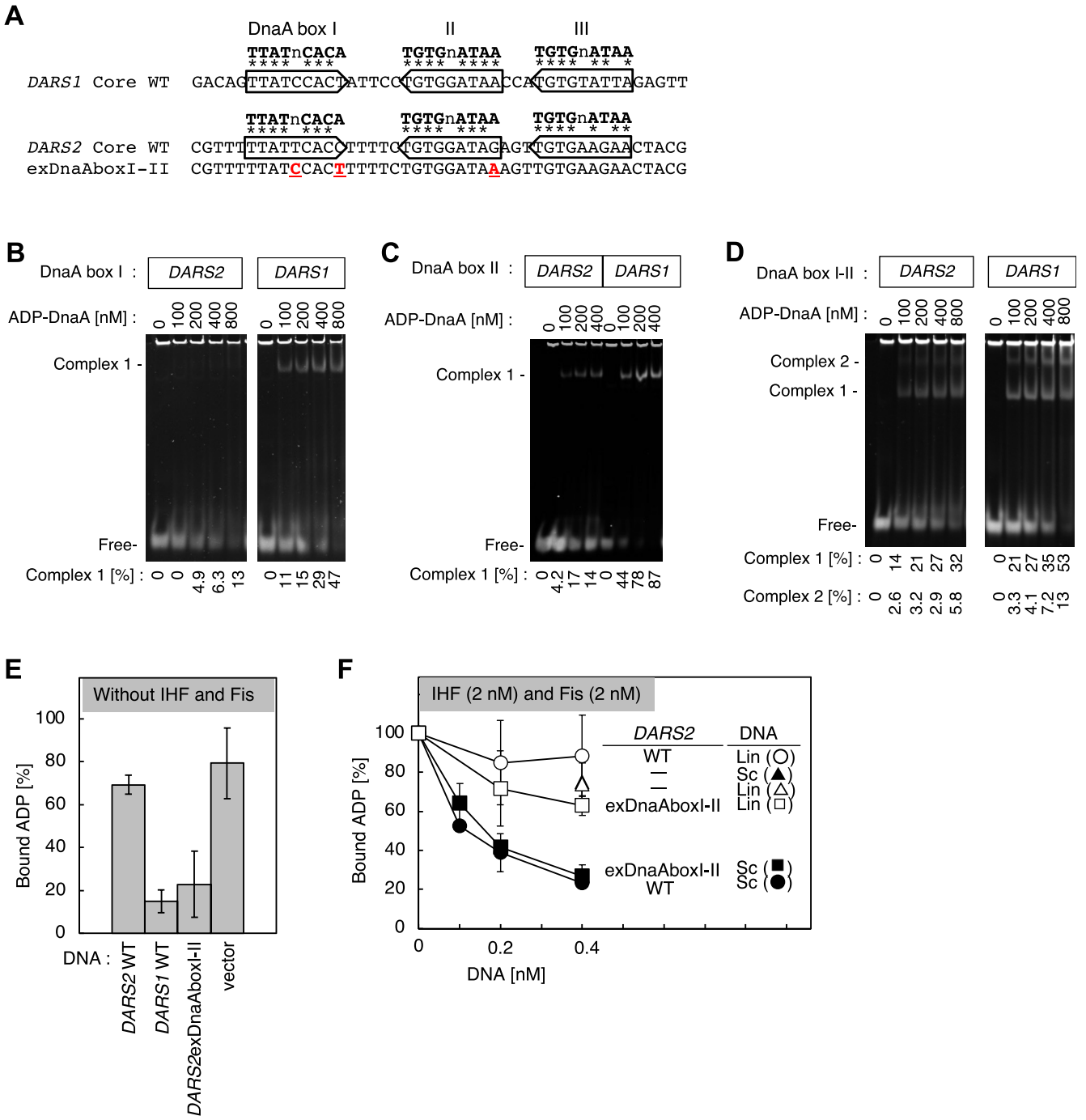

Figure 3. Supercoiling-dependent and independent DnaA-ADP dissociation activity of *DARS2*exDnaAboxI-II. (**A**) Schematic view and sequences of the *DARS2*exDnaAboxI-II mutant. Arrows indicate 9-mer core DnaA boxes of *DARS1* and *DARS2*. Mutated sequence in *DARS2*exDnaAboxI-II mutant is shown with underlines. (**B-D**) ADP-DnaA binding to the core DnaA boxes of *DARS1* and *DARS2*. The indicated amounts of ADP-DnaA were incubated on ice for 5 min with 40 nM of 19-bp dsDNA containing *DARS1* or *DARS2* DnaA box I (**B**), DnaA box II (**C**), or 40 nM of 33-bp dsDNA containing *DARS1* or *DARS2* DnaA boxes I and II (**D**), followed by EMSA with 7% PAGE. Complexes 1 and 2, corresponding to the complexes with one and two molecules of ADP-DnaA, respectively. Free, protein-free DNA. The proportions [%] of Complexes 1 and 2 in each lane are shown below the gel image. (**E, F**) DnaA-ADP dissociation activity of the *DARS2*exDnaAboxes. [^{3}H]ADP-DnaA (80 nM) was incubated at 30°C for 15 min with 2 nM of pOA61 [*DARS2* WT], pOA21 [*DARS1* WT], pKX129 [*DARS2*exDnaAboxI-II] or pACYC177 [vector] (Sc) in the absence of IHF and Fis (**E**), or with indicated amounts of pOA61, pOA21, pKX129 or pACYC177 (Sc or Lin) in the presence of IHF (2 nM as heterodimer) and Fis (2 nM as homodimer) (**F**), followed by the filter binding assay.

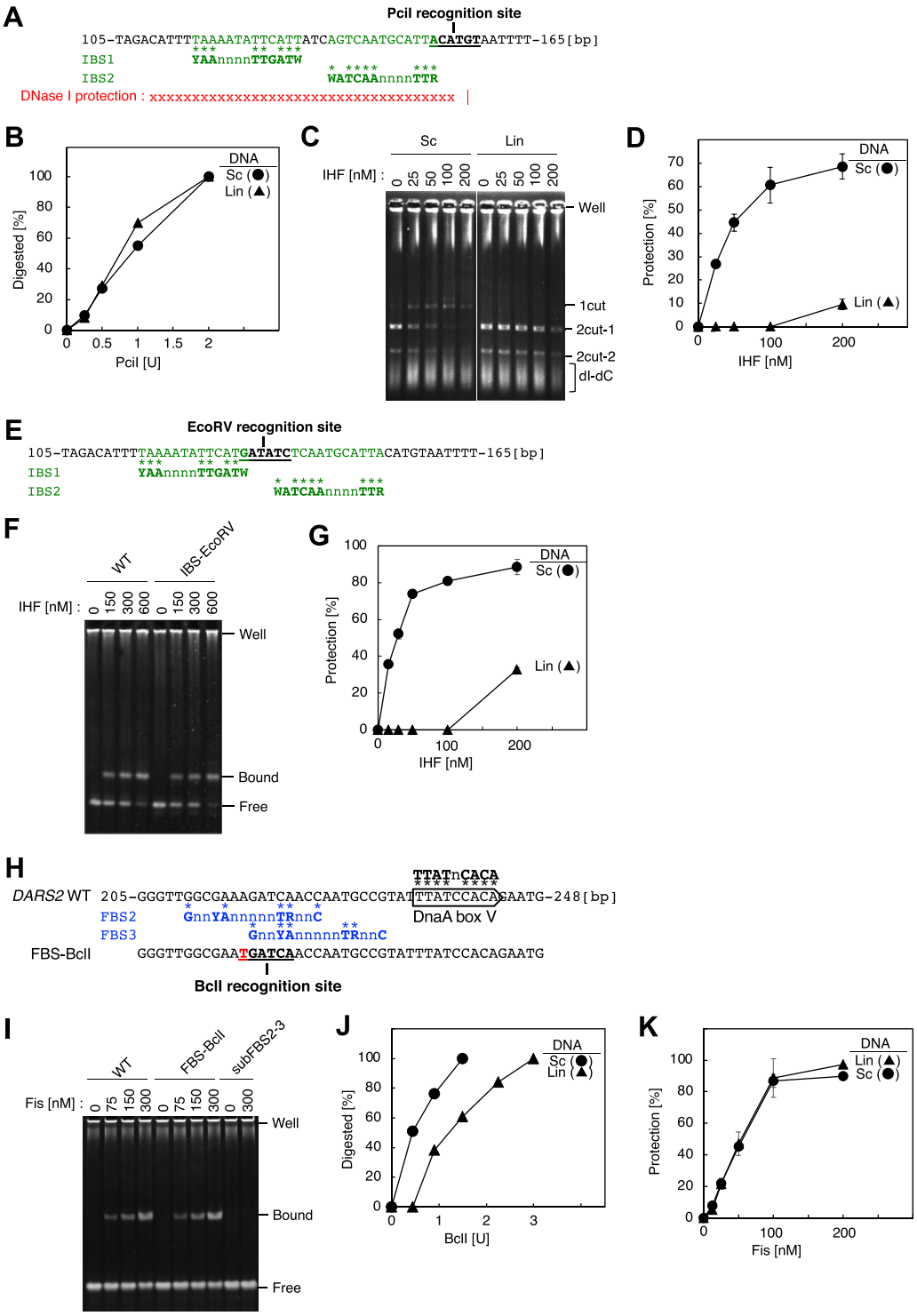

Figure 4. Negative DNA supercoiling is required for stable *DARS2*-IHF binding. (**A**) Primary sequence of the original *DARS2* containing the PciI recognition site located beside the IBS. The DNase I protection sites and hypersensitive sites observed in a previous study are shown as 'x' and '|', respectively (34). (**B**) Effect of the DNA supercoiling on PciI digestion. (**C, D**) PciI protection assay for *DARS2*-IHF binding. The indicated amounts of IHF were incubated at 30°C for 5 min with pOA61 (0.4 nM) and PciI (Sc and Lin; 0.4 units), followed by SacII digestion and agarose gel electrophoresis (**C**). The proportions of undigested DNA to total DNA (Protection) are indicated as percentages (%) (**D**). (**E**) Primary structure of the *DARS2* mutant containing the EcoRV recognition site inside IBS. The underlined characters indicate the EcoRV recognition site, 5′-GATATC-3′. (**F**) IHF binding to the *DARS2* IBS-EcoRV. The indicated amounts of IHF were incubated at 30°C for 5 min with 38-bp dsDNA containing *DARS2* IBS WT or IBS-EcoRV, followed by EMSA with 8% PAGE. (**G**) EcoRV protection assay for *DARS2*-IHF binding. The indicated amounts of IHF were incubated at 30°C for 5 min with pKX137 [*DARS2* IBS-EcoRV] (0.4 nM) and EcoRV (0.5 units). (**H**) Primary structure of the *DARS2* mutant containing BclI-recognition site inside FBS2-3. The underlined characters show the BclI-recognition site, 5′-TGATCA-3′. (**I**) Fis binding to the *DARS2* FBS-BclI. The indicated amounts of Fis were incubated at 30°C for 5 min with 38-bp dsDNA containing *DARS2* FBS WT or FBS-BclI, followed by EMSA with 10% PAGE. (**J**) Check of the DNA supercoiling sensitivity of BclI digestion. (**K**) BclI protection assay for *DARS2*-Fis binding. The indicated amounts of Fis were incubated at 30°C for 5 min with pKX141 [*DARS2* FBS-BclI] (0.4 nM) and BclI (Sc; 1.2 units; Lin; 3.0 units).

Fis directly interacts with DnaA and maximizes *DARS2*-dependent DnaA-ADP dissociation

Based on the observations above, we hypothesized that IHF-dependent DNA loop formation promotes direct interactions between ADP-DnaA oligomers at the *DARS2* core and Fis bound at FBS2-3, which are critical for *DARS2* activation. Previous studies have predicted two protein interaction regions in Fis as follows, which could also be important for its interaction with DnaA; 1) the Fis N-terminal top-loop region (residues 1–26) and 2) the Fis arm-loop region (residues 68–70) positioned adjacent to the helix-turn-helix motif (Figure 5A). To obtain mechanistic insights into Fis-mediated *DARS2* activation, we systematically performed mutational analysis of these Fis residues.

First, we investigated Fis Gln68 and Thr70 residues within the arm-loop regions which directly interact with RNA polymerase α-subunit and stimulate the transcription activity of the *rrnB* P1 promoter (40–42). EMSA experiments using a DNA fragment bearing *DARS2* FBS2-3 confirmed that Fis Q68A and T70A mutants were as effective as Fis WT for binding to *DARS2* FBS2-3 DNA (Figure 5B). In an assay for *DARS2*-dependent DnaA-ADP dissociation in the presence of IHF, Fis Q68A mutant was moderately impaired, whereas Fis T70A mutant was effective as Fis WT (Figure 5C and D). Consistent results were obtained in the time course experiments (Figure 5E). In the presence of Fis WT or Fis T70A mutant, *DARS2* largely dissociated ADP from DnaA within 5 min (Figure 5D), whereas in the presence of Fis Q68A mutant, DnaA-ADP dissociation was impaired and 15 min were required for full dissociation (Figure 5E). *DARS2* activation by Fis Q68A depended on IHF and DNA supercoiling (Figure 5F). Furthermore, protein crosslinking experiments using glutaraldehyde showed that crosslinks between WT Fis and DnaA were detected at a moderate level in the absence of *DARS2* DNA and the Q68A mutation severely inhibited crosslinking with DnaA (Figure 5G), supporting direct and weak interaction of Fis with DnaA in a manner depending on Fis Gln68 residue. These results are consistent with the idea that Fis interacts with DnaA in *DARS2* depending on DNA looping induced by IHF and DNA supercoiling (see 'Discussion' section).

Next, we asked whether the N-terminal top-loop region of Fis is required for *DARS2* activation. Previous reports showed that Fis residues 16–22 within its N-terminal top-loop region directly interact with Hin recombinase in a manner dependent on HU-dependent DNA bending and DNA supercoiling, and promote Hin-dependent DNA inversion activity (43,44). Here, we purified two truncated Fis mutants, Fis Δ16–22 and Δ26, and tested their activities of DNA binding and *DARS2* activation. Figure 5H–K show that Fis Δ16–22 and Δ26 mutants were as effective in binding to DNA and supporting IHF/DNA supercoiling-dependent *DARS2* activation as Fis WT. These support the idea that Fis Gln68 is a specific site important for the *DARS2* activation.

Modulation of DNA supercoiling by Novobiocin diminishes *DARS2* activation by IHF and Fis *in vivo*

To investigate the role of DNA supercoiling in *DARS2* function in cells, we performed flow cytometry analysis to examine the cell cycle parameters of cells growing at 37°C in NaCl-depleted LB medium containing novobiocin, a drug that inhibits DNA gyrase activity and relaxes DNA supercoiling (Figure 6A and B). NaCl depletion commonly induces mild DNA relaxation, and has been used as a standard protocol in combination with novobiocin to induce stronger relaxation of *E. coli* chromosome (45). In exponentially growing *E. coli* cells, replication initiation occurs at sister *oriC* copies synchronously, resulting in the progression of multiple concomitant rounds of replication. Previous studies have indicated that inhibition of the replication initiation by the deletion of *DARS2* core reduces *oriC* copy number in a cell (*oriC*/cells) or in a unit cell mass or cell volume (ori/mass), which are parameters of initiation activity in a cell (46,47). Consistent with these and our previous study (34,48), MIT78 [Δ*DARS2*], MIT17 [Δ*DARS1*], and MIT80 [Δ*DARS1*&*2*] cells exhibited impaired initiation (ori/mass = 0.81 ± 0.03, 0.94 ± 0.04 and 0.66 ± 0.05, respectively), and MIT128 [Δ*datA*] cells exhibited increased initiation (ori/mass = 1.2 ± 0.04), compared with MG1655 [WT] cells (ori/mass = 1 as a standard) (Figure 6B).

Notably, MG1655 cells treated with 15 μg/mL novobiocin showed significant inhibition of initiation (ori/mass = 0.86 ± 0.02), whereas MIT78 [Δ*DARS2*] and MIT80 [Δ*DARS1*&*2*] cells treated with 15 μg/mL novobiocin showed little inhibition of initiation (ori/mass = 0.78 ± 0.03 and 0.71 ± 0.07, respectively): i.e. compare 1 versus 0.86 for WT with or without novobiocin, 0.81 versus 0.78 for Δ*DARS2*, and 0.66 versus 0.71 for Δ*DARS1*&*2* (Figure 6B). By contrast, MIT17 [Δ*DARS1*] and MIT128 [Δ*datA*] cells showed significant novobiocin-dependent inhibition of replication initiation, like MG1655 cells. These results suggest that DNA supercoiling is particularly important for *DARS2* activation in cells. Consistent with the DNA supercoiling requirement for IHF/Fis functions *in vitro*, as well as for the phenotype of Δ*DARS2* cells, the initiation activities of KMG-5 [Δ*ihfA*] and KMG-2 [Δ*fis*] cells were little affected by novobiocin. Consistent results were obtained in the experiments using cells growing in standard LB medium containing 1% NaCl (Supplementary Figure S1), a further support for novobiocin-dependent inhibition of *DARS2* function *in vivo*.

Novobiocin modulates *DARS2*-dependent hydroxyurea sensitivity

A previous study suggested that a reduction in the frequency of replication initiation causes resistance against hydroxyurea, which decreases intracellular dNTP pools and induces replication fork arrest (49). As described in a previous report (50), colony formation by SA102 [Δ*diaA*] cells was resistant to 12.5 mM hydroxyurea (Figure 6C). We also assessed the hydroxyurea sensitivity of MIT17 [Δ*DARS1*], MIT78 [Δ*DARS2*] and MIT80 [Δ*DARS1*&*2*] cells, and obtained the result that colony formation by *DARS* mutant cells was also resistant to 12.5 mM hydroxyurea in a manner correlated with the reduction of initiation frequency (Figure 6B and C). To address the effect of DNA supercoiling on *DARS2*-dependent hydroxyurea sensitivity, we simultaneously added 15 μg/mL novobiocin and 12.5 mM hydroxyurea to the LB plates. Without hydroxyurea, 15 μg/mL novobiocin had little effect on the colony formation of the WT or *DARS* mutant cells. However, addition of 15 μg/mL novobiocin turned MG1655, MIT17 [Δ*DARS1*], and SA102 [Δ*diaA*] colony formation to be resistant to 12.5 mM hydroxyurea, whereas it did not increase the hydroxyurea resistance of MIT78 [Δ*DARS2*] and MIT80

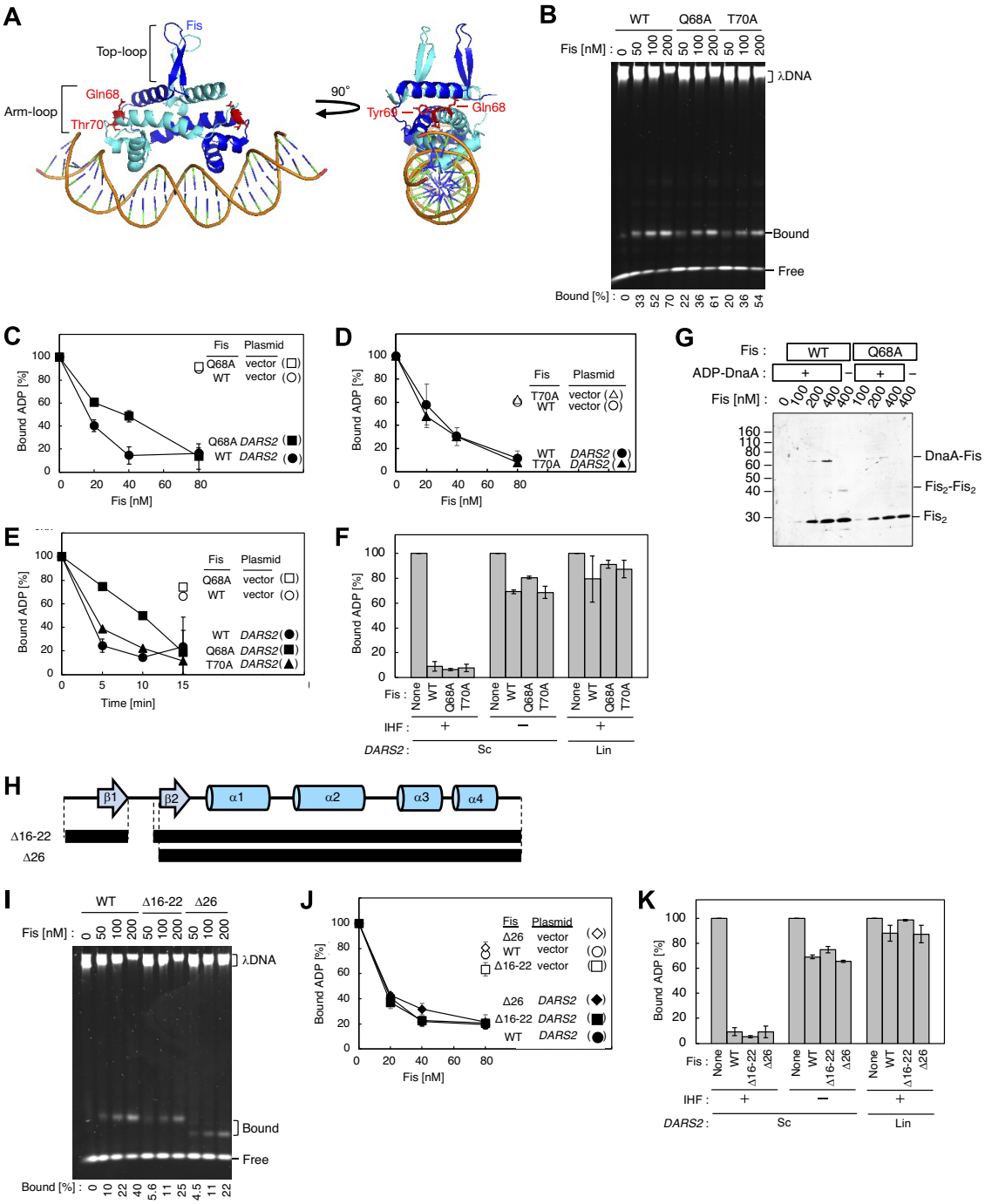

Figure 5. Fis Q68A mutant has decreased activity for *DARS2* activation. (**A**) Structure of Fis-DNA complex. Two potential interaction sites (top-loop and arm-loop) are highlighted; Fis top-loop includes residues 1–26 and Fis arm-loop includes residues 68–70. (**B**) DNA binding activity of Fis Q68A and T70A. The indicated amounts of Fis WT, Q68A, or T70A were incubated with 38-bp dsDNA containing *DARS2* FBS2-3 (40 nM), followed by EMSA with 7% PAGE. The proportions [%] of Fis-bound DNA in each lane are shown below the gel image. (**C-E**) *DARS2* activation by Fis Q68A and T70A. Filter binding assay was performed with [^{3}H]ADP-DnaA (80 nM), 0.4 nM of pOA61 or pACYC177, IHF (2 nM), and the indicated amounts of Fis WT or its mutants (**C**, Q68A; **D**, T70A). Time course experiments were performed at 30°C with 0.4 nM of pOA61 or pACYC177, IHF (2 nM), and Fis WT or its mutants (Q68A or T70A) (2 nM). The proportions [%] of the amounts present in the absence of Fis are plotted. Average values and the standard deviations from three independent experiments are shown (**E**). (**F**) Requirement for DNA supercoiling for *DARS2* activation by Fis Q68A and T70A. [^{3}H]ADP-DnaA (80 nM) was incubated at 30°C for 15 min with IHF (2 nM), Fis WT, Q68A, or T70A (8 nM), and 0.4 nM of supercoiled (Sc) or linear (Lin) pOA61 or pACYC177, followed by the filter binding assay to analyze the yield amount [%] of [^{3}H]ADP-DnaA. (**G**) Dependence of Fis-DnaA interaction on Fis Gln68 residue. ADP-DnaA (100 nM) and indicated amounts of Fis WT or Q68A were incubated at 30°C for 15 min in the presence of 0.1% glutaraldehyde, followed by immunoblotting using anti-Fis antibody. (**H**) Schematic view of the secondary structure of Fis and the truncation mutants constructed in this study. Arrows and cylinders indicate β-strands and α-helixes, respectively. (**I**) DNA binding activity of Fis Δ16–22 and Δ26. EMSA was performed with the indicated amounts of Fis WT, Δ16–22, or Δ26. (**J**) *DARS2* activation by Fis Δ16–22 and Δ26. Filter binding assay was similarly performed with 0.4 nM of pOA61 or pACYC177, IHF (2 nM), and the indicated amounts of Fis WT or mutants (Δ16–22 or Δ26) as dimers. (**K**) Requirement for DNA supercoiling for *DARS2* activation by Fis Δ16–22 and Δ26. [^{3}H]ADP-DnaA (80 nM) was similarly incubated with IHF (2 nM), Fis WT, Δ16–22, or Δ26 (8 nM), and supercoiled (Sc) or linear (Lin) pOA61 or pACYC177 (0.4 nM), followed by the filter binding assay.

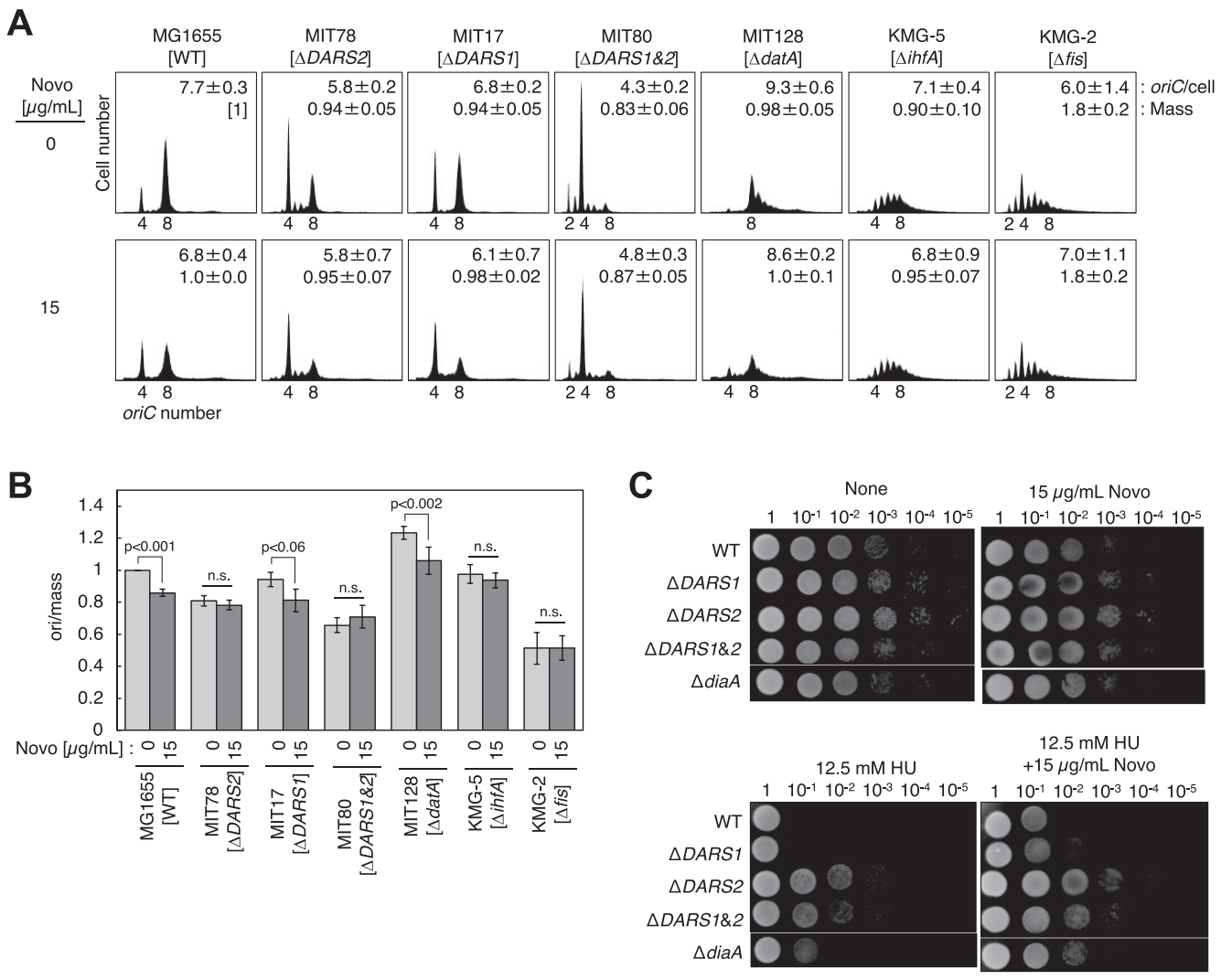

Figure 6. *DARS2* activity is diminished by novobiocin *in vivo*. (**A, B**) Inhibition of *DARS2*/IHF/Fis-dependent stimulation of replication initiation by novobiocin. (**A**) MG1655 [WT], MIT78 [*DARS2*ΔCore], MIT17 [*DARS1*ΔCore], MIT80 [*DARS1*&2ΔCore], MIT128 [Δ*datA*], KMG-5 [Δ*ihfA*] or KMG-2 [Δ*fis*] cells were cultivated at 37°C in NaCl-depleted LB medium containing 0 or 15 μg/mL novobiocin and analyzed by flow cytometry. (**B**) The relative ori/mass ratios (MG1655 cells without novobiocin as a standard) are shown as a bar chart. Data represent means with error bars of at least three independent experiments. Based on the Student's t-test, the comparisons of 15 μg/mL novobiocin versus none of MG1655 ($P < 0.001$), MIT17 ($P < 0.06$) and MIT128 ($P < 0.002$) are statistically significant, whereas those of MIT78, MIT80, KMG-5, KMG-2 were not. (**C**) The effect of novobiocin addition on *DARS2*-dependent hydroxyurea resistance. Serial dilutions of MG1655, MIT78, MIT17, MIT80, MIT128 and SA103 [Δ*diaA*] cells are cultivated at 37°C on LB plates containing novobiocin (0 or 15 μg/mL) and/or hydroxyurea (0 or 12.5 mM) and a spot assay was performed.

[Δ*DARS1*&2] colony formation. These results are consistent with the results of flow cytometry analysis.

Introduction of a *DARS2* mutant harboring *DARS1* core DnaA boxes induces excess and untimely initiation of replication

To investigate whether the *in vivo* activity of *DARS2*exDnaAboxes mutants depends on IHF and Fis (Figures 3A and 7A), we examined the colony formation and timing of replication initiation of MG1655 cells bearing pACYC177 derivatives with *DARS2* WT or *DARS2*exDnaAboxes mutants. Oversupply of *DARS2* WT by pBR322 causes severe inhibition of colony formation due to over-initiation of replication (33). In contrast, copy number of pACYC177 is lower than that of pBR322, and cells bearing pOA61 [*DARS2* WT] grew similarly to cells bearing pACYC177 [Vector] (Figure 7B and C). However, introduction of pKX119 [*DARS2*exCore] or pKX129 [*DARS2*exDnaAboxI-II] in MG1655 cells resulted in severe growth inhibition with formation of colonies only appearing after prolonged incubation (15 h at 37°C). In contrast, introduction of pKX115 [*DARS2*exDnaAboxI], pKX117 [*DARS2*exDnaAboxII], or pKX118 [*DARS2*exDnaAboxIII] resulted in colony formation after 12 h, similar to that of pOA61 [*DARS2* WT] (Figure 7B and C). In addition, introduction of pKX119 [*DARS2*exCore] in KMG-2 [Δ*fis*] or KMG-5 [Δ*ihfA*] cells resulted in colony formation within 12 h (Figure 7D), which is consistent with the data of Figure 3F. These results are consistent with the idea that the *in vivo* activity of *DARS2*exCore and exDnaAboxI-II mutants depends on IHF and Fis, and causes excessive initiations and growth inhibition when the copy number is elevated.

Next, we performed flow cytometry analysis to investigate the cell cycle parameters of MG1655 cells bearing pACYC177 derivatives with *DARS2* WT or *DARS2*exDnaAboxes mutants (Figure 7E and F). In LB medium, introduction of pOA61 [*DARS2* WT] in MG1655 cells stimulated replication initiation and increased the number of cells harboring 16 *oriC*s in a single cell (Figure 7E). Importantly, introduction of pKX115 [*DARS2*exDnaAboxI] or pKX117 [*DARS2*exDnaAboxII] resulted in even higher *oriC* copy numbers (Figure 7E). In contrast, introduction of pKX118 [*DARS2*exDnaAboxIII] resulted in *oriC* copy numbers comparable to that of pOA61 [*DARS2* WT]. Similar results were obtained when cells were cultivated in supplemented M9 medium (Figure 7F). Also, the results were consistent with those of flow cytometry analysis of MG1655 cells bearing pACYC177 derivatives with *DARS1*ex mutants, and introduction of pKX110 [*DARS1*exDnaAboxI], pKX111 [*DARS1*exDnaAboxII], or pKX114 [*DARS1*exCore] diminished the activity for increasing the initiation frequency (Supplementary Figure S2). In contrast, that of pKX113 [*DARS1*exDnaAboxIII] resulted in *oriC* copy numbers comparable to that of pOA21 [*DARS1* WT]. These results suggest that core DnaA box I and II, but not III, are required for efficient DnaA activation by *DARS1*, and *DARS2*exDnaAboxI and II mutants stimulate initiation in cells more than *DARS1/2* WT.

The cell cycle parameters (*oriC*/cell, ori/mass ratios, and Ai: asynchrony index) were also analyzed in cells with chromosomal *DARS2*exDnaAboxes mutants (Figure 7G). The Ai (asynchronous index) evaluates the level of untimely initiations, and, in MG1655 cells, the Ai value was very low (Ai = 6.5%), which means that replication was initiated profoundly synchronously. In KX219 [*DARS2*exDnaAboxII] cells, the Ai value was increased (Ai = 22%) and the number of *oriC* copies per cell (*oriC*/cell) and initiation frequency (ori/mass) were also increased (*oriC*/cell = 4.6, ori/mass = 1.1) relative to those in MG1655 cells (*oriC*/cell = 4.0, ori/mass = 1 as a standard) (Figure 7G). Furthermore, KX221 [*DARS2*exCore] and KX222 [*DARS2*exDnaAboxI-II] cells have higher *oriC* copy numbers (*oriC*/cell = 5.5 or 5.4, respectively) and severe asynchronous initiation (Ai = 139% or 119%, respectively), indicating that chromosomal *DARS2*exDnaAboxes mutants induce excess and untimely initiations.

Next, to investigate the contribution of DNA supercoiling to *DARS2*exCore function in cells, we performed flow cytometry analysis on cells growing at 37°C in NaCl-depleted LB medium containing 15 μg/mL novobiocin. Consistent with the results shown in Figure 7G, KX221 [*DARS2*exCore] cells showed more initiations (ori/mass = 1.2 ± 0.06) than MG1655 cells (ori/mass = 1 as a standard) (Figure 7H and I). Notably, KX216 cells treated with 15 μg/mL novobiocin showed significant inhibition of initiation (ori/mass = 1.1 ± 0.08), which was comparable to that of MG1655 cells treated with novobiocin (ori/mass = 0.89 ± 0.06), suggesting that activation of the *DARS2*exCore mutant also requires DNA supercoiling *in vivo*.

Discussion

ATP-DnaA production from ADP-DnaA is largely achieved by the timely binding of both IHF and Fis to *DARS2* (34,37). This study provides direct evidence that stable *DARS2*-IHF binding and DnaA-ADP dissociation by *DARS2*–IHF–Fis complex are stimulated by negative DNA supercoiling (Figures 2 and 4). Consistently, the function of chromosomal *DARS2* in growing cells is inhibited by novobiocin (Figure 6). A previous study probing the genome-wide dynamics of DNA supercoiling using psoralen, a supercoiling-sensitive DNA intercalator, has suggested that negative DNA supercoiling locally accumulates at the genomic *DARS2* locus (51). Based on these, we suggest a possibility that dynamic changes in chromosomal DNA supercoiling at *DARS2* locus is a potential regulatory element for the timely *DARS2*-IHF binding during cell cycle (Figure 8A). In addition, salt depletion in LB medium also alters the ATP/ADP ratio in the *E. coli* cells, and affects the activity of DNA gyrase, an ATP-dependent type II topoisomerase, resulting in mitigation of genomic DNA supercoiling (52,53). Based on these and this study, we suggest a possibility that *DARS2* function is regulated depending on growth environments through modulation of DNA supercoiling.

Previous studies employing EMSA or DNase I footprinting showed IHF bound to linear *DARS2* under mild salt conditions (100 mM potassium glutamate, equivalent to 60 mM NaCl) (34,54); however, high IHF concentrations were needed for the binding under these conditions; i.e. 20–40 IHF dimers/1 kb DNA were required to achieve 50% binding to linear *DARS2*, whereas in the present study, 10–15 IHF dimers/1 kb DNA were sufficient to achieve 50% binding to supercoiled *DARS2* under near-physiological salt conditions (100 mM NaCl). Also, IHF hardly protected linear *DARS2* from restriction enzyme digestion, indicating that DNA supercoiling converts the *DARS2*-IHF complex into one that is more stable and resistant against salt and competitive proteins. A previous report showed that DNA supercoiling also stabilizes *datA*-IHF binding under high salt stress (31). Molecular dynamics simulations have also supported our findings that DNA supercoiling affects DNA recognition by IHF and increases IHF wrapping around DNA (55). The preferential binding to supercoiled or curved DNA rather than to straight DNA is a universal feature of bacterial NAPs, including IHF, an IHF homologue HU, and a DNA-bridging factor H-NS, (38,56–60). Furthermore, the eukaryotic high mobility group family protein Abf2, a yeast mitochondrial counterpart of NAPs, as well as archaebacterial histone-like protein MC1, also have higher affinity for supercoiled DNA than for relaxed DNA (61,62). DNA supercoiling-dependent regulation of protein binding to DNA is universally conserved in a broad range of species.

The IHF binding pattern at *oriC* is also changed during the *E. coli* cell cycle. During the cell cycle, IHF binds to *oriC* specifically at the stage of replication initiation and dissociates from *oriC* immediately after initiation (30,63,64). Further characterization of the genomic pattern of IHF binding has provided evidence for the uniqueness and specificity of IHF binding at *oriC*. At the initiation stage, IHF recognizes a 33-mer initiation-specific IHF binding consensus sequence 1-GTTGnnGnnnWnnAAAnnCAnnnnTTTnWnAAC-33 that consists of the core DNA elements 19-CA-20 and 25-TT-26, which are conserved together with the conventional IBS consensus WATCAAnnnnTTR, as well as unique surrounding elements 1-GTTG-4 and 31-AAC-33 (64). Profiling of IHF consensus binding sequences has suggested that IHF binding affinity for each IBS depends on surrounding

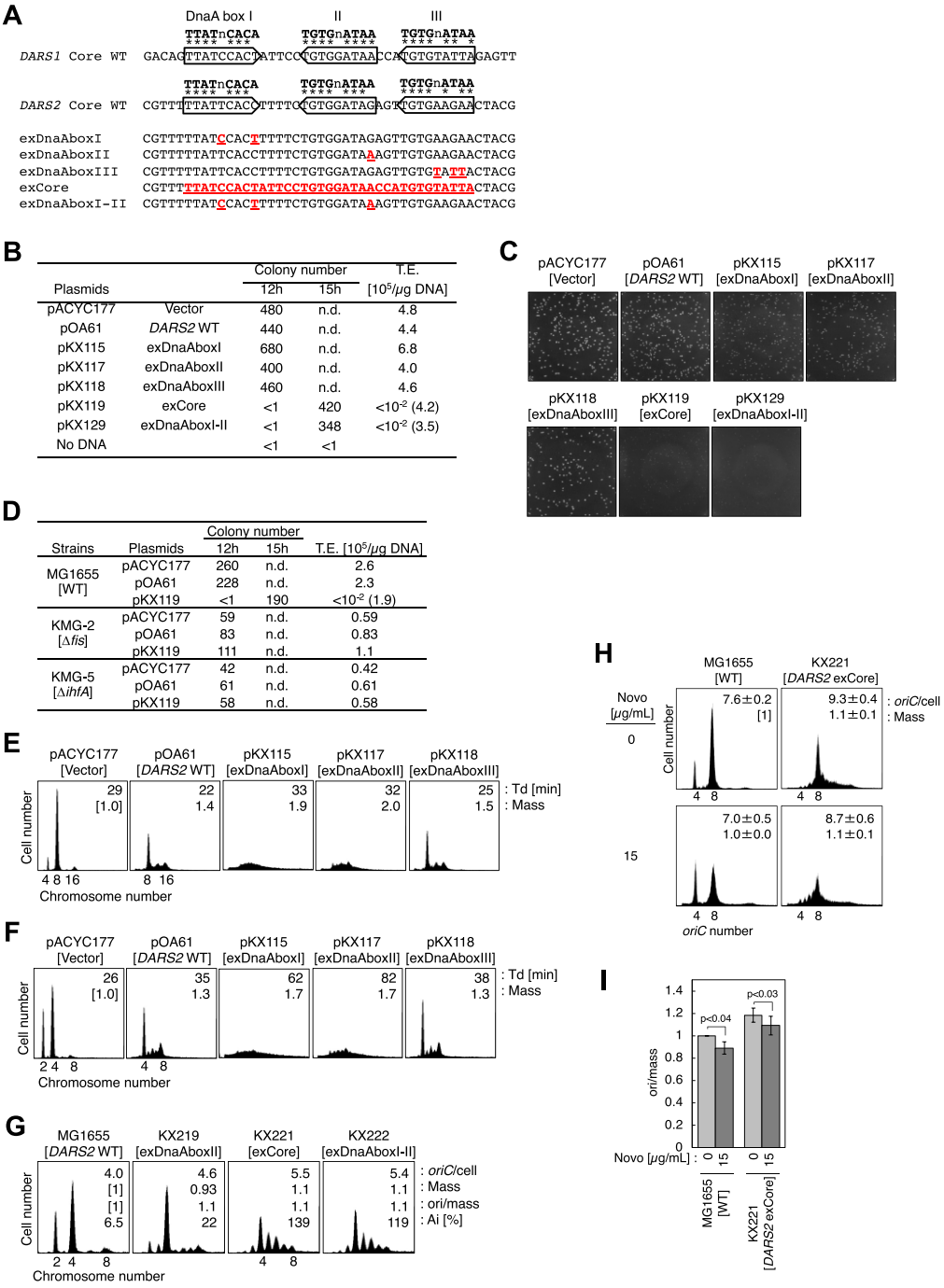

Figure 7. *DARS2*exDnaAboxes mutants cause excess and untimely initiation. (**A**) schematic view and sequences of the *DARS2*exDnaAboxes mutants. Arrows indicate 9-mer core DnaA boxes of *DARS1* and *DARS2*. Mutated sequences in *DARS2*exDnaAboxes mutants (*DARS2* exDnaAboxI, exDnaAboxII, exDnaAboxIII, exCore, and exDnaAboxI-II) are shown with underlines. (B-C) Growth inhibition by the oversupply of *DARS2*exDnaAboxes mutant. MG1655 cells were transformed with pACYC177 [vector], pOA61 [*DARS2* WT], pKX115 [*DARS2*exDnaAboxI], pKX117 [*DARS2*exDnaAboxII], pKX118 [*DARS2*exDnaAboxIII], pKX119 [*DARS2*exCore] or pKX129 [*DARS2*exDnaAboxI-II] and incubated at 37°C for 12 h on LB agar plates containing 100 μg/mL ampicillin. The number of transformants and the efficiency of transformation (T.E. [10^5/μg DNA]) (**B**), and colony formation with each set of experiments (**C**) are shown. (**D**) Suppression of *DARS2*exDnaAboxes-dependent growth inhibition by deletion of IHF/Fis. MG1655, KMG-2 or KMG-5 cells were transformed with pACYC177, pOA61 or pKX119 and incubated at 37°C for 12 h on LB agar plates containing 100 μg/mL ampicillin. (**E-G**) *DARS2*exDnaAboxes-dependent over-initiations. (**E**) MG1655 cells harboring pACYC177, pOA61, pKX115, pKX117 or pKX118 were cultivated at 37°C in LB medium containing 50 μg/mL ampicillin and analyzed by flow cytometry. The doubling time (Td [min]) and mean cell mass (relative to MG1655 cells harboring pACYC177) are shown in the histograms. (**F**) Similar experiments were performed using supplemented M9 medium containing 50 μg/mL ampicillin. (**G**) MG1655 [WT], KX219 [*DARS2*exDnaAboxII], KX221 [*DARS2*exCore] or KX222 [*DARS2*exDnaAboxI-II] cells were cultivated at 37°C in supplemented M9 medium and analyzed by flow cytometry. The *oriC*/cell, mean cell mass, ori/mass (relative to MG1655 cells), and Ai [%] are shown in the histograms. (**H, I**) Inhibition of *DARS2*exCore activity by novobiocin. (**H**) MG1655 and KX221 cells were cultivated at 37°C in NaCl-depleted LB medium containing 0 or 15 μg/mL novobiocin and analyzed by flow cytometry. (**I**) The relative ori/mass ratio (MG1655 cells without novobiocin were used as the control) are shown as a bar chart. Data represent means with error bars from three independent experiments. Based on the Student's t-test, the comparisons of the 15 μg/mL novobiocin versus none of MG1655 ($P < 0.04$) and KX221 ($P < 0.03$) are both statistically significant.

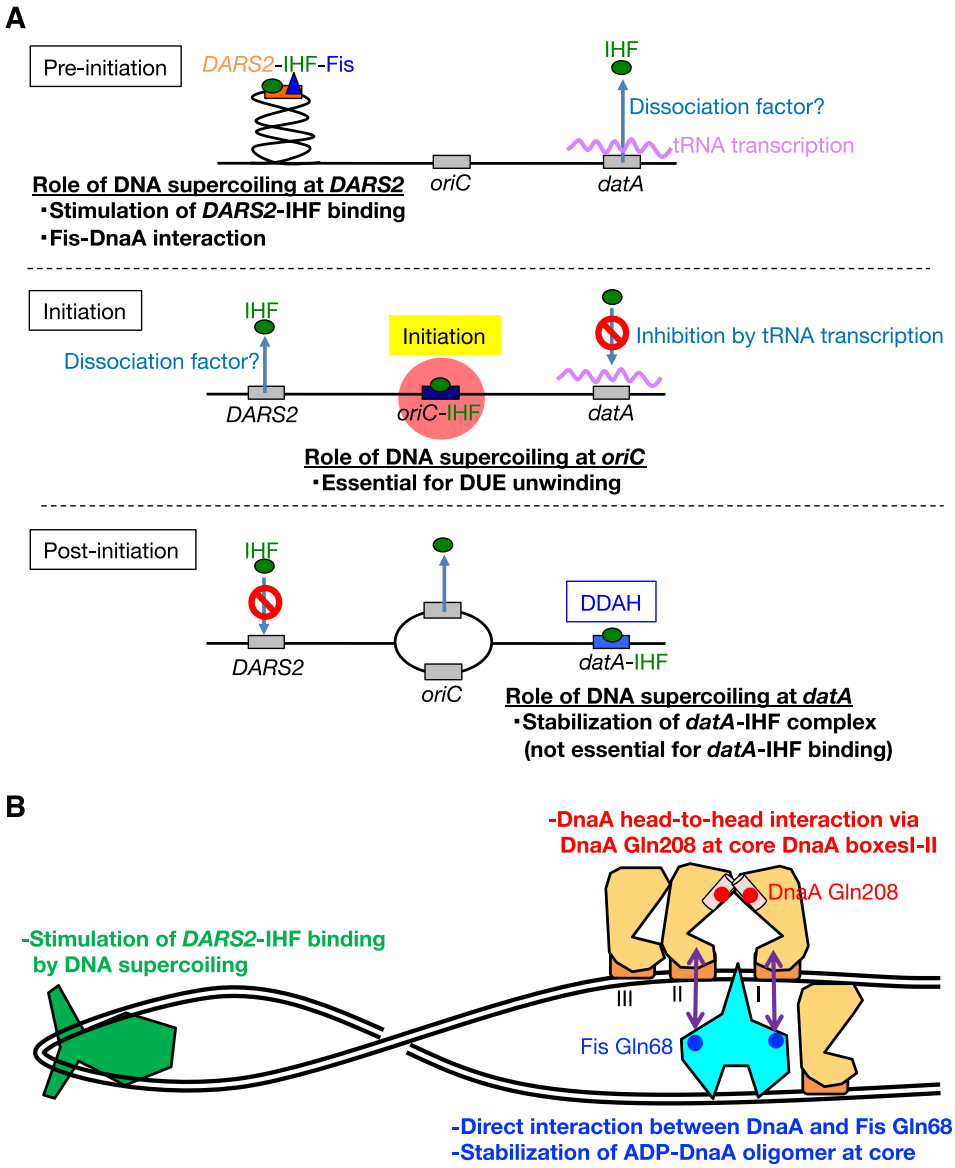

Figure 8. Timely regulation and mechanism of DNA supercoiling-dependent *DARS2* activation. (**A**) A model of the DNA supercoiling-dependent regulation of *DARS2*-IHF binding. In the pre-initiation stage, IHF binds to *oriC* and *DARS2* and the *DARS2*–IHF-Fis complex increases the level of ATP-DnaA. At the initiation stage, IHF dissociates from *DARS2* and the elevated ATP-DnaA level induces initiation from *oriC*. In the post-initiation stage, IHF immediately dissociates from *oriC* and binds to *datA* to activate DDAH. IHF then dissociates from *datA* in a manner dependent on tRNA-Gly transcription readthrough. (**B**) Mechanistic model of *DARS2* activation by IHF, Fis, and DNA supercoiling. ADP-DnaA, IHF and Fis bind to specific sites. IHF stably binds to *DARS2* IBS1-2 and forms a stable DNA loop in a manner dependent on DNA supercoiling, which induces direct interaction between Fis Glu68 and the head-to-head DnaA dimer formed at core DnaA boxes I-II, resulting in a structural change in the DnaA nucleotide-binding pocket and dissociation of ADP from DnaA (not directly shown in this study).

AT-rich elements (8). Local DNA looping is induced at the *oriC* IBS1 by the assembly of DUE-proximal ATP-DnaA oligomers, which is also important for HU-dependent stimulation of *oriC* DUE unwinding (38). The induced DNA bending at the *oriC* IBS1 recruits HU, which further stimulates DUE unwinding in the *oriC*-DnaA-HU complexes, similar to IHF binding. In this context, we propose that at specific cell cycle stages, a DNA supercoiling-dependent genome structuring or local DNA looping may increase dependency on surrounding DNA elements at the *DARS2* IBS for stabilizing IHF binding.

Another potential regulatory mechanism could be a synergy between the effects of IHF and Fis. This study revealed that only *DARS2*-IHF binding, but not *DARS2*-Fis binding, was dependent on DNA supercoiling (Figure 4). A previous systematic study using synthetic transcriptional promoters revealed that Fis binding to a specific locus can alter the transcription activity by changing the specificity of IHF-DNA binding (65). Also, simultaneous binding of IHF and Fis can synergistically activate transcription activity, which is consistent with the ideas that DNA bending by IHF allows Fis to interact physically with its interacting partners, such as RNA polymerase and DnaA, to stimulate transcription initiation or to dissociate DnaA-ADP at *DARS2*. Previous studies also reported that Fis dissociates from *DARS2* at the time of IHF dissociation (34,37), implying another possible effect of IHF-Fis synergy to monitor *DARS2*-IHF for-

mation or dissociation by Fis at specific times during the cell cycle.

About the mechanism for *DARS2* activation by Fis, this study revealed that the Fis Q68A mutant was not as effective as Fis WT for *DARS2* activation (Figure 5C and E). A previous study suggested that Fis stimulates ADP-DnaA assembly at the *DARS2* core (34). In addition, this study has suggested that the Fis Gln68 residue at the arm-loop region (residues 68–74), which is required for interaction with RNA polymerase α-subunit (40), is also required for direct interaction with DnaA (Figure 5G). Based on these observations, we propose a novel mechanistic model for *DARS2* activation in which direct DnaA-Fis interaction stimulates the ADP-DnaA oligomerization at the *DARS2* core to induce the conformational change in the DnaA nucleotide-binding pocket required for ADP dissociation (Figure 8B).

Also, this study revealed that the *DARS1* core contains high affinity DnaA boxes I and II, whereas the *DARS2* core contains only low affinity ones (Figure 3B-D). The head-to-head ADP-DnaA dimer was less stable at *DARS2* than at *DARS1*, which is consistent with the idea that Fis supports ADP-DnaA oligomerization at the *DARS2* core (Figure 8B). When the head-to-head ADP-DnaA dimer bound to core DnaA boxes I and II is stabilized at a certain level, interaction between the two via DnaA AAA + domain III Gln208 would become functional to induce a structural change in the DnaA protomers of the dimer and ADP dissociation as we previously proposed (Figure 1G) (35). In agreement, the core DnaA box III of *DARS1* and *DARS2*, which is essential for their activity, supports DnaA head-to-tail interaction via DnaA AID-2 (Leu290) residue to stabilize head-to-head DnaA interaction at core DnaA boxes I and II (Figure 1G) (35). These DnaA box III sequences are functionally inter-changeable between *DARS1* and *DARS2*, suggesting the presence of a common mechanism (Figure 7E and F and Supplementary Figure S2). Taken together, the head-to-head ADP-DnaA dimer formed at the *DARS* core would have to be stable at a certain level for the ADP dissociation in both *DARS1* and *DARS2*.

The essential elements of *DARS2* (core DnaA boxes I-III, IBS, and FBS) are well conserved among *E. coli*-related bacteria (34). Also, *Vibrio cholerae* harbors specific non-coding DNA element *crtS* for regulating the activity of RctB for initiating Chr2 replication (66). And in eukaryotes, the initiator complex ORC (Origin recognition complex), which consists of five AAA + family or AAA+-like subunits (Orc1–5) and one regulatory subunit Orc6, binds to specific chromosomal replication origins and initiates replication (67,68). The initiation activity of ORC is commonly regulated by its bound nucleotides (ATP or ADP) and phosphorylation of its constituent proteins. In *Saccharomyces cerevisiae*, ORC forms a homomultimer on single-stranded DNA, stimulating ORC ATPase activity (69). ssDNA-dependent ORC regulation may be required to repress over-initiation, suggesting that DNA-mediated regulation of the ORC nucleotide form by its self-oligomerization may be conserved in other eukaryotic cells. Other reports have suggested that *S. cerevisiae* ORC interacts with the nucleosome specifically at the replication origin, ARS1 (70–72). Unlike DnaA in *E. coli*, *Drosophila melanogaster* ORC has been reported to have a 30-fold higher affinity for supercoiled DNA than for linear one (73). Although *DARS2*-like sequences have not been reported in eukaryotic genomes, these studies implies that histone- or DNA supercoiling-dependent regulations of initiator binding at specific genomic loci and the nucleotide form could be conserved among eukaryotes for the regulation of the timing of replication initiation.

Data availability

The data supporting the findings of this study are available from the corresponding author upon reasonable request.

Supplementary data

Supplementary Data are available at NAR Online.

Acknowledgements

We are grateful to Dr. Kazuyuki Fujimitsu for the initial analysis of supercoiled *DARS2* DNA.

Funding

Japan Society for the Promotion of Science (JSPS KAKENHI) [JP20H03212, JP21K19233 and JP23K27131]; Gushinkai [2023 Samuro Kakiuchi Memorial Research Award for Young Scientists].

Conflict of interest statement

None declared

References

1. Molan,K. and Žgur Bertok,D. (2022) Small prokaryotic DNA-binding proteins protect genome integrity throughout the life cycle. *Int. J. Mol. Sci.*, **23**, 4008.
2. Hołówka,J. and Zakrzewska-Czerwińska,J. (2020) Nucleoid associated proteins: the small organizers that help to cope with stress. *Front. Microbiol.*, **11**, 590.
3. Dillon,S.C. and Dorman,C.J. (2010) Bacterial nucleoid-associated proteins, nucleoid structure and gene expression. *Nat. Rev. Microbiol.*, **8**, 185–195.
4. Frimodt-Møller,J., Charbon,G. and Løbner-Olesen,A. (2017) Control of bacterial chromosome replication by non-coding regions outside the origin. *Curr. Genet.*, **63**, 607–611.
5. Grimwade,J.E. and Leonard,A.C. (2021) Blocking, bending, and binding: regulation of initiation of chromosome replication during the *Escherichia coli* cell cycle by transcriptional modulators that interact with origin DNA. *Front. Microbiol.*, **12**, 732270.
6. Kasho,K., Ozaki,S. and Katayama,T. (2023) IHF and Fis as *Escherichia coli* cell cycle regulators: activation of the replication origin *oriC* and the regulatory cycle of the DnaA initiator. *Int. J. Mol. Sci.*, **24**, 11572.
7. Rice,P.A., Yang,S., Mizuuchi,K. and Nash,H.A. (1996) Crystal structure of an IHF-DNA complex : a protein-induced DNA U-turn. *Cell*, **87**, 1295–1306.
8. Aeling,K.A., Opel,M.L., Steffen,N.R., Tretyachenko-Ladokhina,V., Hatfield,G.W., Lathrop,R.H. and Senear,D.F. (2006) Indirect recognition in sequence-specific DNA binding by *Escherichia coli* integration host factor: the role of DNA deformation energy. *J. Biol. Chem.*, **281**, 39236–39248.
9. Katayama,T., Ozaki,S., Keyamura,K. and Fujimitsu,K. (2010) Regulation of the replication cycle: conserved and diverse regulatory systems for DnaA and *oriC*. *Nat. Rev. Microbiol.*, **8**, 163–170.

10. Katayama,T., Kasho,K. and Kawakami,H. (2017) The DnaA cycle in *Escherichia coli*: activation, function and inactivation of the initiator protein. *Front. Microbiol.*, **8**, 2496.
11. Hansen,F.G. and Atlung,T. (2018) The DnaA tale. *Front Microbiol.*, **9**, 319.
12. Chodavarapu,S. and Kaguni,J.M. (2016) Replication initiation in bacteria. *Enzym*, **39**, 1–30.
13. Abe,Y., Jo,T., Matsuda,Y., Matsunaga,C., Katayama,T. and Ueda,T. (2007) Structure and function of DnaA N-terminal domains: specific sites and mechanisms in inter-DnaA interaction and in DnaB helicase loading on *oriC*. *J. Biol. Chem.*, **282**, 17816–17827.
14. Keyamura,K., Abe,Y., Higashi,M., Ueda,T. and Katayama,T. (2009) DiaA dynamics are coupled with changes in initial origin complexes leading to helicase loading. *J. Biol. Chem.*, **284**, 25038–25050.
15. Zawilak-Pawlik,A., Nowaczyk,M. and Zakrzewska-Czerwińska,J. (2017) The role of the N-terminal domains of bacterial initiator DnaA in the assembly and regulation of the bacterial replication initiation complex. *Genes (Basel).*, **8**, 136.
16. Nozaki,S. and Ogawa,T. (2008) Determination of the minimum domain II size of *Escherichia coli* DnaA protein essential for cell viability. *Microbiology*, **154**, 3379–3384.
17. Fujikawa,N., Kurumizaka,H., Nureki,O., Terada,T., Shirouzu,M., Katayama,T. and Shigeyuki,Y. (2003) Structural basis of replication origin recognition by the DnaA protein. *Nucleic Acids Res.*, **31**, 2077–2086.
18. Noguchi,Y., Sakiyama,Y., Kawakami,H. and Katayama,T. (2015) The arg fingers of key DnaA protomers are oriented inward within the replication origin *oriC* and stimulate DnaA subcomplexes in the initiation complex. *J. Biol. Chem.*, **290**, 20295–20312.
19. Sakiyama,Y., Kasho,K., Noguchi,Y., Kawakami,H. and Katayama,T. (2017) Regulatory dynamics in the ternary DnaA complex for initiation of chromosomal replication in *Escherichia coli*. *Nucleic Acids Res.*, **45**, 12354–12373.
20. Saxena,R., Vasudevan,S., Patil,D., Ashoura,N., Grimwade,J.E. and Crooke,E. (2015) Nucleotide-induced conformational changes in *Escherichia coli* DnaA protein are required for bacterial ORC to pre-RC conversion at the chromosomal origin. *Int. J. Mol. Sci.*, **16**, 27897–27911.
21. Hwang,D.S. and Kornberg,A. (1992) Opening of the replication origin of *Escherichia coli* by DnaA protein with Protein HU or IHF. *J. Biol. Chem.*, **267**, 23083–23086.
22. Ozaki,S., Kawakami,H., Nakamura,K., Fujikawa,N., Kagawa,W., Park,S.-Y., Yokoyama,S., Kurumizaka,H. and Katayama,T. (2008) A common mechanism for the ATP-DnaA-dependent formation of open complexes at the replication origin. *J. Biol. Chem.*, **283**, 8351–8362.
23. Sakiyama,Y., Nagata,M., Yoshida,R., Kasho,K., Ozaki,S. and Katayama,T. (2022) Concerted actions of DnaA complexes with DNA-unwinding sequences within and flanking replication origin *oriC* promote DnaB helicase loading. *J. Biol. Chem.*, **298**, 102051.
24. Duderstadt,K.E., Chuang,K. and Berger,J.M. (2011) DNA stretching by bacterial initiators promotes replication origin opening. *Nature*, **478**, 209–213.
25. Kurokawa,K., Nishida,S., Emoto,A., Sekimizu,K. and Katayama,T. (1999) Replication cycle-coordinated change of the adenine nucleotide-bound forms of DnaA protein in *Escherichia coli*. *EMBO J.*, **18**, 6642–6652.
26. Katayama,T., Kubota,T., Kurokawa,K., Crooke,E. and Sekimizu,K. (1998) The initiator function of DnaA protein is negatively regulated by the sliding clamp of the *E. coli* chromosomal replicase. *Cell*, **94**, 61–71.
27. Kato,J. and Katayama,T. (2001) Hda, a novel DnaA-related protein, regulates the replication cycle in *Escherichia coli*. *EMBO J.*, **20**, 4253–4262.
28. Baxter,J.C. and Sutton,M.D. (2012) Evidence for roles of the *Escherichia coli* Hda protein beyond regulatory inactivation of DnaA. *Mol. Microbiol.*, **85**, 648–668.
29. Kim,J.S., Nanfara,M.T., Chodavarapu,S., Jin,K.S., Babu,V.M.P., Ghazy,M.A., Chung,S., Kaguni,J.M., Sutton,M.D. and Cho,Y. (2017) Dynamic assembly of Hda and the sliding clamp in the regulation of replication licensing. *Nucleic Acids Res.*, **45**, 3888–3905.
30. Kasho,K. and Katayama,T. (2013) DnaA binding locus *datA* promotes DnaA-ATP hydrolysis to enable cell cycle-coordinated replication initiation. *Proc. Natl. Acad. Sci. USA*, **110**, 936–941.
31. Kasho,K., Tanaka,H., Sakai,R. and Katayama,T. (2017) Cooperative DnaA binding to the negatively supercoiled *datA* locus stimulates DnaA-ATP hydrolysis. *J. Biol. Chem.*, **292**, 1251–1266.
32. Kasho,K., Sakai,R., Ito,K., Nakagaki,W., Satomura,R., Jinnouchi,T., Ozaki,S. and Katayama,T. (2024) Read-through transcription of tRNA underlies the cell cycle-dependent dissociation of IHF from the DnaA-inactivating sequence *datA*. *Front. Microbiol.*, **15**, 1360108.
33. Fujimitsu,K., Senriuchi,T. and Katayama,T. (2009) Specific genomic sequences of *E. coli* promote replicational initiation by directly reactivating ADP-DnaA. *Genes Dev.*, **23**, 1221–1233.
34. Kasho,K., Fujimitsu,K., Matoba,T., Oshima,T. and Katayama,T. (2014) Timely binding of IHF and Fis to *DARS2* regulates ATP-DnaA production and replication initiation. *Nucleic Acids Res.*, **42**, 13134–13149.
35. Sugiyama,R., Kasho,K., Miyoshi,K., Ozaki,S., Kagawa,W., Kurumizaka,H. and Katayama,T. (2019) A novel mode of DnaA-DnaA interaction promotes ADP dissociation for reactivation of replication initiation activity. *Nucleic Acids Res.*, **47**, 11209–11224.
36. Stella,S., Cascio,D. and Johnson,R.C. (2010) The shape of the DNA minor groove directs binding by the DNA-bending protein Fis. *Genes Dev.*, **24**, 814–826.
37. Miyoshi,K., Tatsumoto,Y., Ozaki,S. and Katayama,T. (2021) Negative feedback for *DARS2*–Fis complex by ATP–DnaA supports the cell cycle-coordinated regulation for chromosome replication. *Nucleic Acids Res.*, **49**, 12820–12835.
38. Yoshida,R., Ozaki,S., Kawakami,H. and Katayama,T. (2023) Single-stranded DNA recruitment mechanism in replication origin unwinding by DnaA initiator protein and HU, an evolutionary ubiquitous nucleoid protein. *Nucleic Acids Res.*, **51**, 6286–6306.
39. Datsenko,K.A. and Wanner,B.L. (2000) One-step inactivation of chromosomal genes in *Escherichia coli* K-12 using PCR products. *Proc. Natl. Acad. Sci. USA*, **97**, 6640–6645.
40. Bokal,A.J., Ross,W., Gaal,T., Johnson,R.C. and Gourse,R.L. (1997) Molecular anatomy of a transcription activation patch: FIS-RNA polymerase interactions at the *Escherichia coli rrnB* P1 promoter. *EMBO J.*, **16**, 154–162.
41. Aiyar,S.E., McLeod,S.M., Ross,W., Hirvonen,C.A., Thomas,M.S., Johnson,R.C. and Gourse,R.L. (2002) Architecture of Fis-activated transcription complexes at the *Escherichia coli rrnB* P1 and rrnE P1 promoters. *J. Mol. Biol.*, **316**, 501–516.
42. Zhi,H., Wang,X., Cabrera,J.E., Johnson,R.C. and Jin,D.J. (2003) Fis stabilizes the interaction between RNA polymerase and the ribosomal promoter *rrnB* P1, leading to transcriptional activation. *J. Biol. Chem.*, **278**, 47340–47349.
43. Dhar,G., Heiss,J.K. and Johnson,R.C. (2009) Mechanical constraints on Hin subunit rotation imposed by the Fis/enhancer system and DNA supercoiling during site-specific recombination. *Mol. Cell*, **34**, 746–759.
44. McLean,M.M., Chang,Y., Dhar,G., Heiss,J.K. and Johnson,R.C. (2013) Multiple interfaces between a serine recombinase and an enhancer control site-specific DNA inversion. *eLife*, **2**, e01211.
45. Cameron,A.D.S., Stoebel,D.M. and Dorman,C.J. (2011) DNA supercoiling is differentially regulated by environmental factors and FIS in *Escherichia coli* and *Salmonella enterica*. *Mol. Microbiol.*, **80**, 85–101.
46. Skarstad,K., Løbner-Olesen,A., Atlung,T., von Meyenburg,K. and Boye,E. (1989) Initiation of DNA replication in *Escherichia coli*

after overproduction of the DnaA protein. *Mol. Gen. Genet.*, **218**, 50–56.
47. Weigel,C., Messer,W., Preiss,S., Welzeck,M.,,Morigen and Boye,E. (2001) The sequence requirements for a functional *Escherichia coli* replication origin are different for the chromosome and a minichromosome. *Mol. Microbiol.*, **40**, 498–507.
48. Inoue,Y., Tanaka,H., Kasho,K., Fujimitsu,K., Oshima,T. and Katayama,T. (2016) Chromosomal location of the DnaA-reactivating sequence *DARS2* is important to regulate timely initiation of DNA replication in *Escherichia coli*. *Genes Cells*, **9**, 1015–1023.
49. Sutera,V.A.J. and Lovett,S.T. (2006) The role of replication initiation control in promoting survival of replication fork damage. *Mol. Microbiol.*, **60**, 229–239.
50. Noguchi,Y. and Katayama,T. (2016) The *Escherichia coli* cryptic prophage protein YfdR binds to DnaA and initiation of chromosomal replication is inhibited by overexpression of the gene cluster *yfdQ-yfdR-yfdS-yfdT*. *Front. Microbiol.*, **7**, 239.
51. Pham,P., Wood,E.A., Dunbar,E.L., Cox,M.M. and Goodman,M.F. (2024) Controlling genome topology with sequences that trigger post-replication gap formation during replisome passage: the *E. coli* RRS elements. *Nucleic Acids Res.*, **52**, 6392–6405.
52. Hsieh,L.S., Rouviere-Yaniv,J. and Drlica,K. (1991) Bacterial DNA supercoiling and [ATP]/[ADP] ratio: changes associated with salt shock. *J. Bacteriol.*, **173**, 3914–3917.
53. Jensen,P.R., Loman,L., Petra,B., Van der Weijden,C. and Westerhoff,H.V. (1995) Energy buffering of DNA structure fails when *Escherichia coli* runs out of substrate. *J. Bacteriol.*, **177**, 3420–3426.
54. Leirmo,S., Harrison,C., Cayley,D.S., Burgess,R.R. and Record,M.T.J. (1987) Replacement of potassium chloride by potassium glutamate dramatically enhances protein-DNA interactions *invitro*. *Biochemistry*, **26**, 2095–2101.
55. Watson,G.D., Chan,E.W., Leake,M.C. and Noy,A. (2022) Structural interplay between DNA-shape protein recognition and supercoiling: the case of IHF. *Comput. Struct. Biotechnol. J.*, **20**, 5264–5274.
56. Shindo,H., Furubayashi,A., Shimizu,M., Miyake,M. and Imamoto,F. (1992) Preferential binding of *E.coli* histone-like protein HU alpha to negatively supercoiled DNA. *Nucleic Acids Res.*, **20**, 1553–1558.
57. Dame,R.T., Wyman,C. and Goosen,N. (2001) Structural basis for preferential binding of H-NS to curved DNA. *Biochimie*, **83**, 231–234.
58. Huang,L., Zhang,Z. and McMacken,R. (2021) Interaction of the *Escherichia coli* HU protein with various topological forms of DNA. *Biomolecules*, **11**, 1724.
59. Teter,B., Goodman,S.D. and Galas,D.J. (2000) DNA bending and twisting properties of integration host factor determined by DNA cyclization. *Plasmid*, **84**, 73–84.
60. Swinger,K. and Rice.,P. (2004) IHF and HU : flexible architects of bent DNA. *Curr. Opin. Struct. Biol.*, **14**, 28–35.
61. Teyssier,C., Toulme,F., Touzel,J., Gervais,A. and Maurizot,J. (1996) Preferential binding of the archaebacterial histone-like MC1 protein to negatively supercoiled DNA minicircles. *Biochemistry*, **2960**, 7954–7958.
62. Diffley,J.F. and Stillman,B. (1992) DNA binding properties of an HMG1-related protein from yeast mitochondria. *J. Biol. Chem.*, **267**, 3368–3374.
63. Cassler,M.R., Grimwade,J.E. and Leonard,A.C. (1995) Cell cycle-specific changes in nucleoprotein complexes at a chromosomal replication origin. *EMBO J.*, **14**, 5833–5841.
64. Kasho,K., Oshima,T., Chumsakul,O., Nakamura,K., Fukamachi,K. and Katayama,T. (2021) Whole-genome analysis reveals that the nucleoid protein IHF predominantly binds to the replication origin *oriC* specifically at the time of initiation. *Front. Microbiol.*, **12**, 697712.
65. Monteiro,L.M.O., Sanches-Medeiros,A., Westmann,C.A. and Silva-Rocha,R. (2020) Unraveling the complex interplay of fis and IHF through synthetic promoter engineering. *Front. Bioeng. Biotechnol.*, **8**, 510.
66. Doan,A., Chatterjee,S., Kothapalli,R., Khan,Z., Sen,S., Kedei,N., Jha,J.K., Chattoraj,D.K. and Ramachandran,R. (2024) The replication enhancer *crtS*depends on transcription factor Lrp for modulating binding of initiator RctB to *ori*2 of *Vibrio cholerae*. *Nucleic Acids Res.*, **52**, 708–723.
67. Hu,Y. and Stillman,B. (2023) Origins of DNA replication in eukaryotes. *Mol. Cell*, **83**, 352–372.
68. Costa,A. and Diffley,J.F.X. (2022) The initiation of eukaryotic DNA replication. *Annu. Rev. Biochem.*, **91**, 107–131.
69. Kawakami,H., Muraoka,R., Ohashi,E., Kawabata,K., Kanamoto,S., Chichibu,T., Tsurimoto,T. and Katayama,T. (2019) Specific basic patch-dependent multimerization of *Saccharomycescerevisiae* ORC on single-stranded DNA promotes ATP hydrolysis. *Genes Cells*, **24**, 608–618.
70. Müller,P., Park,S., Shor,E., Huebert,D.J., Warren,C.L., Ansari,A.Z., Weinreich,M., Eaton,M.L., MacAlpine,D.M. and Fox,C.A. (2010) The conserved bromo-adjacent homology domain of yeast Orc1 functions in the selection of DNA replication origins within chromatin. *Genes Dev.*, **24**, 1418–1433.
71. Hizume,K., Yagura,M. and Araki,H. (2013) Concerted interaction between origin recognition complex (ORC), nucleosomes and replication origin DNA ensures stable ORC-origin binding. *Genes Cells*, **18**, 764–779.
72. Li,S., Wasserman,M.R., Yurieva,O., Bai,L., O'Donnell,M.E. and Liu,S. (2022) Nucleosome-directed replication origin licensing independent of a consensus DNA sequence. *Nat. Commun.*, **13**, 4947.
73. Remus,D., Beall,E.L. and Botchan,M.R. (2004) DNA topology, not DNA sequence, is a critical determinant for Drosophila ORC-DNA binding. *EMBO J.*, **23**, 897–907.

Received: August 9, 2024. **Revised:** December 13, 2024. **Editorial Decision:** December 13, 2024. **Accepted:** December 19, 2024